Eur. Phys. J. C (2020) 80:818
https://doi.org/10.1140/epjc/s10052-020-8368-x

THE EUROPEAN PHYSICAL JOURNAL C

Regular Article - Theoretical Physics

Stop search in SUSY SO(10) GUTs with nonuniversal Gaugino masses

Zafer Altın[a], **Zerrin Kırca**[b], **Tuğçe Tanımak**[c], **Cem Salih Ün**[d]

Department of Physics, Bursa Uludağ University, 16059 Bursa, Turkey

Received: 10 March 2020 / Accepted: 17 August 2020 / Published online: 4 September 2020

Abstract We explore the stop mass and its possible probe through a set of three different signal processes within a class of SUSY GUTs with non-universal gaugino masses. The stop mass can be realized in a wide range (0.4–8 TeV) consistent with the current experimental constraints. We consider the decay processes; $\tilde{t}_1 \to t\tilde{\chi}_1^0, \tilde{t}_1 \to bW^{\pm}\tilde{\chi}_1^0$ and $\tilde{t}_1 \to bq\bar{q}'\tilde{\chi}_1^0$ to be possible signals, and explore the impact of the current experimental results as well as the possible mass scales of stop, which can be probed in the future collider experiments. We find that the first and third signal processes can be tested in the current experiments, and significantly probed in future, while the second signal process is not available for the current experiments in this class of SUSY GUTs. We also comment that the second signal process can be available to be tested when the collider experiments are conducted at high center of mass energies and luminosity.

1 Introduction

The standard model (SM) of the elementary particles is one of the most successful theory in physics, and its glory was embraced especially after the Higgs boson discovery by the ATLAS [1] and CMS [2] experiments. Despite its success and good agreement between its predictions and the experimental results, the SM can only be an effective theory due to its problematic structure for the Higgs boson. The most significant problem raises in stabilizing the Higgs boson mass against the quadratic divergent radiative contributions, which is very well-known as the gauge hierarchy problem [3–7]. Besides, the SM with a 125 GeV Higgs boson loses the absolute stability of the Higgs potential [8–10] at some high scale, which may bring another reason for the need of models beyond the SM. As one of the forefront candidates, the supersymmetric models can resolve the gauge hierarchy problem by extending the SM with superpartners such that the quadratic divergences in the Higgs boson mass are canceled. Besides, imposing the conservation of $R-$parity requires the lightest supersymmetric particle (LSP) to be stable, and neutral weakly interacting supersymmetric particles can provide pleasant dark matter (DM) candidates. In addition, the minimal supersymmetric extension of the SM (MSSM) almost unifies the three SM gauge couplings, even though it preserves the SM gauge symmetry. Together with stabilizing the Higgs boson mass at all energy scales, the gauge coupling unification motivates the supersymmetric grand unified theories (SUSY GUTs), and one can explore implications of GUTs at the electroweak scale by linking the high scale origin to the weak scale observables through the renormalization group equations (RGEs), which has allowed to explore the implications of GUTs based on SU(5) [11–21] or SO(10) [22–52].

Even though the experimental observations and constraints from the Higgs boson searches (see, for instance, [53–75]) point a need for new physics, and the observations can be accommodated in SUSY GUTs [76–84], absence of a direct signal in the experiments brings a strong impact in searches for the new physics. As is a hadron collider, the LHC results are quite effective, especially on new colored particles such as gluino and stop in the SUSY models. Even though it depends on the decay modes of the gluino and the mass scale of the LSP neutralino, the current LHC results set a bound on the gluino mass as $m_{\tilde{g}} \geq 2.1$ TeV [85,86]. This bound reduces as $m_{\tilde{g}} \gtrsim 800$ GeV, when the gluino happens to be next to LSP (NLSP). A recent study has shown that these bounds can also be employed in the electroweak scale mass spectra of SUSY GUTs [87].

Contributing through RGEs heavy gluino mass scales exclude the stop solutions lighter than about 400 GeV in the MSSM framework [87]. A further exclusion on the stop mass

[a] e-mail: 501407009@ogr.uludag.edu.tr
[b] e-mail: zkirca@uludag.edu.tr
[c] e-mail: 501807001@ogr.uludag.edu.tr
[d] e-mail: cemsalihun@uludag.edu.tr (corresponding author)

can be obtained by performing collider analyses over the possible decay modes of the stop. The most stringent exclusion on the stop mass arises, if the stop decays into a top quark and a LSP neutralino. Results from the ATLAS and CMS experiments [88] exclude the solutions with $m_{\tilde{t}_1} \lesssim 1200$ GeV. Nature of the LSP also takes part in analyses such that if the Higgsinos take part in forming the LSP, then the exclusion happens as $m_{\tilde{t}_1} \gtrsim 900$ GeV [89]. Besides, the number of leptons in the final states can lower the exclusion as $m_{\tilde{t}_1} \gtrsim 800$ GeV [90]. Similar results can be obtained if the stop is allowed to decay into a chargino along with a bottom quark, which resumes on the chargino decay into a LSP neutralino and a $W-$boson. The analyses over such events exclude the solutions with $m_{\tilde{t}_1} \lesssim 1100$ GeV [88,91]. The lowest bound on the stop mass is obtained when the stop can decay only into a LSP neutralino along with a charm quark. This decay mode is not very exclusive due to the soft charm jets and low missing energy [92]. Such events exclude the stop mass as $m_{\tilde{t}_1} \lesssim 550$ GeV [93].

Most of these analyses, on the other hand, are mostly performed in the electroweak scale MSSM framework. They assume specific configurations on the mass differences among the relevant particles, 100% branching ratios for the decay modes under concern, largest production cross-section etc. In addition, rest of the supersymmetric mass spectrum is assumed to be heavy enough not to interfere in the events. Such configurations are very common and can be easily adjusted, since MSSM has more than a hundred parameters including masses, mixings, soft supersymmetry breaking (SSB) trilinear couplings and so on. On the other hand, if one considers the electroweak scale implications of a class of SUSY GUTs, then some of the configurations may not be possible, since a quite large number of observables are calculated in terms of a few free parameters. For instance, when the stop is allowed to decay into a top quark and a LSP neutralino, a class of SUSY GUTs with non-universal gaugino masses (NUGM) at the grand unification scale ($M_{\rm GUT}$) can yield an exclusion at about 50% Confidence Level (CL), at most, in the region with $m_{\tilde{t}_1} \lesssim 500$ GeV (see, for instance, Refs. [94,95]), even though the analyses in MSSM exclude the same region at 95% CL [89,90].

In this work, we simulate the similar analyses of signal-background comparisons in the framework of SUSY GUTs with non-universal gaugino masses at the GUT scale. The rest of the paper is organized as follows: We discuss some salient features of $SO(10)$ SUSY GUTs in Sect. 2. Section 3 describes the scanning procedure and the experimental constraints employed in our analyses. Also we define the signal strength and confidence level (CL) in this section. We discuss the mass spectrum and the availability of the signal processes in Sect. 4, and we quantitatively present our results for the exclusion curves for the stop mass scales in the current experiments in Sect. 5. We also show our results for probing the stop mass in future experiments through the possible signal processes in this section. Finally, we summarize and conclude our findings in Sect. 6.

2 Supersymmetric $SO(10)$ with non-universal Gauginos

In this section, we describe some of the salient features of $SO(10)$ SUSY GUTs, and summarize its building blocks, which are relevant in our analyses. One of the main motivations in $SO(10)$ SUSY GUTs is the matter unification, in addition to the gauge coupling unification. The spinor representation in $SO(10)$ GUTs is 16 dimensional, and all the matter fermions of a family along with a right-handed neutrino can fit into a single multiplet (16_i). The presence of a right-handed neutrino per family helps to implement seesaw mechanism for tiny neutrino masses (see, for instance, [96–103]) as well as it can account for the baryon asymmetry of the Universe through leptogenesis (see, for instance, [104–110]).

In addition, a minimal setup allows one to reside the two MSSM Higgs doublets in one 10 dimensional representation of the $SO(10)$ group, which leads to combine all the Yukawa interactions into a single term in the superpotential as $Y_{ij}16_i16_j10_H$, where i, j are the family indices, and subscript H indicates the 10-plet of the MSSM Higgs fields. This feature of minimal $SO(10)$ SUSY GUTs yields Yukawa unification (YU) at the GUT scale that can be expressed as

$$Y_u = Y_d = Y_e = Y_\nu \tag{1}$$

where Y_u and Y_d denote the Yukawa matrices for up-type and down-type quarks, respectively, while Y_e shows that of the charged leptons. Since $SO(10)$ spinor representation includes a right-handed neutrino, its Yukawa matrix, Y_ν should also be involved in the Yukawa unification scheme. YU faces two difficulties in satisfying the consistent lepton and quark masses. First difficulty is encountered to include the neutrino Yukawa coupling. A sizeable neutrino Yukawa coupling ($Y_\nu = \mathcal{O}(1)$) requires the right handed neutrino masses to be $M_{N_R} \sim 10^{14} - 10^{15}$ GeV [111], while a consistent leptogenesis requires $M_{N_R} \sim 10^9 - 10^{10}$ GeV which yields $Y_\nu \sim 10^{-3}$ [112]. Furthermore, if one considers TeV scale right-handed neutrinos, then the consistent neutrino masses requires $Y_\nu \lesssim 10^{-7}$ [113]. Apparently, it is not easy to involve such a small neutrino Yukawa coupling in the YU scheme together with the other Yukawa couplings. Note that if one implements inverse seesaw mechanism [114,115], then a sizeable neutrino Yukawa coupling can be realized even if the right-handed neutrinos have a TeV scale masses [116]. In this case, one can propose approximate YU [117].

However, one should notice the second difficulty is severer than the one mentioned above, since YU fails to satisfy consistent fermion masses. It predicts $N = U \propto D = L$, where N, U, D, L denote the Dirac mass matrices of right-handed neutrino, up-type and down-type quarks, charged leptons, respectively. $U \propto D$ implies vanishing quark flavor mixing [118]. Besides, since it sets $D = L^T$, YU also leads to the naive SU(5) relations among the asymptotic masses as $m_b = m_\tau$, $m_s = m_\mu$ and $m_d = m_e$. While the renormalization group (RG) evolution can yield consistent bottom and tau masses at the weak scale, the other two strongly disagree with the experimental measurements on the fermion masses. One way to resolve this discrepancy is to add more Higgs fields from different representations of $SO(10)$ [119]. While the contradictory mass relations can be avoided with more Higgs fields, the unification of the Yukawa couplings is lost, since the MSSM Higgs doublets are, in general, superpositions of the Higgs fields from different representations. Even though YU can be maintained for the third family through some assumptions, we do not consider them in our work.

These Higgs fields from different representations can also trigger the $SO(10)$ breaking. A large variety of different Higgs representations can be employed in the $SO(10)$ breaking path. For instance, one can consider the following superpotential involving the Higgs fields from 10, 45 and 16 representations:

$$\mathcal{L} \supset Y_{ij} 16_i 16_j 10_H + \sum_a Y'^{(a)}_{ij} 16_i 16_j \left(\frac{45^a_H}{M}\right) 10_H + Y''_{ij} \frac{16_i 16_j 16^{(1)}_H 16^{(1)}_H}{M} \tag{2}$$

where, i, j indices represent the matter families, while H means the multiplet of the Higgs fields. M is a scale associated with the effective non-renormalizable interactions. In principle, one can have several 45−dimensional Higgs representations distinguished with the upper index a. If we consider two 45 of the Higgs fields, then one 45 can develop vacuum expectation values (VEVs) in $B-L$ direction, while the other does to break I_{3R}. Breaking of the $B-L$ symmetry in this way yields correct mass relations between the down-type quarks and charged leptons in the first and second families [120]. In addition, I_{3R} breaking through the VEV of a second 45_H breaks the proportionality $U \propto D$ and leads to the correct CKM matrix. The non-zero VEVs in $\overline{16}$ can generate heavy right-handed neutrino masses. In addition, their VEVs reduce the rank from 5 to 4, which induces extra $D-$term contribution to the masses of the scalar matter fields [121–125]. We use an upper index (1) for 16_H, since we are not restricted to include only one 16_H representation. Indeed, one can also consider a second Higgs multiplet ($16^{(2)}_H$) as

$$\mathcal{L} \supset Y''_{ij} \frac{16_i 16_j 16^{(1)}_H 16^{(1)}_H}{M} + Y'''_{ij} \frac{16_i 16_j 16^{(2)}_H 16^{(2)}_H}{M} \tag{3}$$

The $B-L$ symmetry can be broken through VEVs of $SU(5)$ singlet Higgs fields in these representations. If the MSSM Higgs doublets are assumed to be included in these 16_H representations, then extracting two light Higgs doublet after the symmetry breaking requires a complicated GUT spectrum for the Higgs fields involving, for instance, one of each 54_H and 45_H, and three 10_H [126]. On the other hand, one can follow the $SO(10)$ breaking through VEVs from two 45_H representations, and keep two 16_H for rank reduction, while the MSSM Higgs fields are kept in a 10_H. In this case, the $D-$term contribution to the scalar masses will be proportional to $M_{X^{(1)}} - M_{X^{(2)}}$, where $X^{(1,2)}$ are the Higgs fields from $16^{(1,2)}_H$, respectively, and $M_{X^{(i)}}$ denote their soft masses. An approximate equality between their soft masses yields negligible $D-$term contributions to the SSB masses of the scalar matter fields (see, for instance, [127]).

The consistent fermion masses can be obtained through renormalizable couplings if the superpotential involves the Higgs fields from 10_H, 120_H and 126_H [128] as;

$$\mathcal{L} \supset 16_i \left(\sum_a Y^a 10^a_H + \sum_b Y'^b 120^b_H + \sum_c Y''^c 126^c_H \right) 16_j \tag{4}$$

where a, b, c denote the number of the Higgs representations. In addition to these fields, we can have other Higgs fields from a 210_H representation, but since these fields do not have Yukawa coupling to the matter fields at the renormalizable level, we assume they take part in symmetry breaking only. Even though only one representation from each in Eq. (4) will be enough for the consistent fermion masses, we assume there are two 126_H representations to complete the symmetry breaking. In this setup, the $SO(10)$ symmetry can be broken as follows:

$$\begin{aligned} SO(10) &\xrightarrow{\mathbf{210}} SU(4) \times SU(2)_L \times SU(2)_R \\ &\xrightarrow{\mathbf{126} \oplus \overline{\mathbf{126}}} SU(3)_c \times SU(2)_L \times U(1)_Y \end{aligned} \tag{5}$$

where the role of $\overline{\mathbf{126}}$ is to cancel the $D-$term contributions. The following chain is also possible.

$$\begin{aligned} SO(10) &\xrightarrow{\mathbf{210}} SU(3)_c \times SU(2)_L \times U(1)_Y \times U(1)_{B-L} \\ &\xrightarrow{\mathbf{126} \oplus \overline{\mathbf{126}}} SU(3)_c \times SU(2)_L \times U(1)_Y \end{aligned} \tag{6}$$

Unification of the matter fields of a family requires the same SSB mass terms for these fields. However, it does not have to imply any relation among the mass terms associated with different families. Indeed, the restrictions on the SSB masses come from the experimental results. For instance, a consistent $K - \bar{K}$ mixing requires $m_{\tilde{d}} = m_{\tilde{s}}$ [129], and it yields the same SSB masses for the first and second matter families in the $SO(10)$ SUSY GUTs. The universality in

the first and second family masses can be considered as the presence of a flavor symmetry at the GUT scale [130–132]. Even though, one can adjust different masses for the families along with a flavor symmetry, we will assume all three families have the same SSB masses at the GUT scale. Besides, as discussed above, we assume $D-$flat directions in $SO(10)$ breaking such that the SSB masses of the scalar matter fields do not receive $D-$term contributions.

The SSB gaugino masses in gravity mediated SUSY breaking can be generated by a VEV of an auxiliary field F through dimension 5 operators as [133–136]

$$-\frac{F^{ab}}{M_P}\lambda^a\lambda^b \xrightarrow{\langle F\rangle \neq 0} -M^{ab}_{1/2}\lambda^a\lambda^b \tag{7}$$

Supersymmetric generalization of dimension 5 operators can be obtained if F^{ab} belongs to the symmetric part of direct product of the adjoint representation of the GUT symmetry group [137] that is for $SO(10)$:

$$(45\times 45)_S = 1 + 54 + 210 + 770 \tag{8}$$

If F belongs to the singlet representation, then the SUSY breaking generates universal gaugino masses. On the other hand, there are some other F fields in the other representations shown in the right hand side of Eq. (8), which are singlet under the MSSM gauge group. If the SUSY is broken by VEVs of multiple F fields from different representations, then the gauginos receive different SSB masses from the SUSY breaking [138–142]. In addition, there could be more representations, in which $\langle F\rangle$ can generate different gaugino masses, if one considers different embedding of $SO(10)$ into E_6 group (for more details, please see [140]). In this work, we consider the case in which SUSY might be broken through VEVs of an arbitrary combination of F fields from different representations such as those in Eq. (8), which results in independent non-universal SSB mass terms for the gauginos.

Despite a variety of different breaking patterns of $SO(10)$ symmetry which may yield different extensions of MSSM, most of them lead to similar implications when one considers the masses, decay channels and possible signals for the stop and gluino [143–146]. Even though they can yield LSPs other than MSSM neutralinos [147–151], stop and gluino either do not directly decay into such LSPs [152] or they do interact very weakly [153]. Unless the stop is NLSP, the neutralino more likely participates in the possible stop signals, and if the neutralino travels longer than about 1 millimeter before decaying into the LSP, then the missing energy in the signals arises due to the missing neutralinos [153]. If the stop or gluino happens to be NSLP and directly decay into the LSP, then they usually become long-lived particles, and the limits on their mass scales are already stronger than those set in the neutralino LSP cases [154,155].

On the other hand a $SO(10)$ SUSY GUT model can be distinguished from those classified in $SU(5)$ GUTs. Since the gauge coupling unification can be maintained with a relatively light color triplet in $SU(5)$, it yields a proton lifetime about 10^4 times shorter than the experimental constraints [156]. This issue in $SU(5)$ can be resolved when the mass spectrum is very heavy, which involves the superpartners of mass beyond TeV scales. Even though small $\tan\beta$ values may allow relatively lighter decoupling scale for the supersymmetric particles, it is still beyond 100 TeV, and it becomes much higher even when $\tan\beta \sim 30$ [157]. Defining the decoupling scale as $M_{\rm SUSY} = \sqrt{m_{\tilde{t}_L} m_{\tilde{t}_R}}$ a high decoupling scale leads to very heavy stops, which are beyond the reach of the current and future collider experiments.

In our work, we consider the possible stop signals in a class of $SO(10)$ SUSY GUTs, in which the MSSM Higgs fields are solely involved in a 10_H representation, while there are more Higgs fields from different representations to break the $SO(10)$ symmetry such that the $D-$term contributions to the matter scalars are canceled. Thus, we impose universal SSB mass terms for the supersymmetric matter particles, while the gauginos have non-universal SSB masses at the GUT scale. Even though the MSSM Higgs fields have different masses based on the discussion of possible Higgs sector in the $SO(10)$ SUSY GUTs, we set their masses equal to the masses of the scalar matter fields for simplicity, since the implications about the possible stop signals are not very sensitive to the SSB masses of the MSSM Higgs fields at the GUT scale.

3 Scanning procedure and experimental constraints

We have employed SPheno 4.0.3 package [158,159] generated with SARAH 4.13.0 [160,161]. In this package, the weak scale values of the gauge and Yukawa couplings in MSSM are evolved to the unification scale $M_{\rm GUT}$ via the renormalization group equations (RGEs). $M_{\rm GUT}$ is determined by the requirement of unification of the gauge couplings through their RGE evolutions. Note that we do not strictly enforce the unification condition $g_1 = g_2 = g_3$ at $M_{\rm GUT}$ since a few percent deviation from the unification can be assigned to unknown GUT-scale threshold corrections [162,163]. Afterwards, the boundary conditions are implemented at $M_{\rm GUT}$ and all the SSB parameters along with the gauge and Yukawa couplings are evolved back to the weak scale by employing two-loop RGEs.

We performed random scans in the fundamental parameter space of NUGM, in which each set of input values is represented by a vector, whose components correspond to the free parameters of NUGM as listed below with their ranges;

$$\begin{aligned} 0 \leq & \quad m_0 \quad \leq 5 \text{ TeV}, \\ 0 \leq & \quad M_1, M_2, M_3 \leq 5 \text{ TeV}, \\ -3 \leq & \quad A_0/m_0 \quad \leq 3, \\ 1.2 \leq & \quad \tan\beta \quad \leq 60. \end{aligned} \tag{9}$$

where m_0 is the universal SSB mass term for the matter scalars and Higgs fields. M_1, M_2 and M_3 are the SSB mass terms for the gauginos associated with the $U(1)_Y$, $SU(2)_L$ and $SU(3)_C$ symmetry groups respectively. A_0 is the SSB trilinear coupling, and $\tan\beta$ is ratio of VEVs of the MSSM Higgs doublets. Finally, we have used the central value of top quark mass, $m_t = 173.3$ GeV [164]. Note that the sparticle spectrum is not too sensitive for one or two sigma variation in the top quark mass [165], but it can shift the Higgs boson mass by 1-2 GeV [166,167].

The radiative electroweak symmetry breaking (REWSB) condition provides a strict theoretical constraint [168–172] over the fundamental parameter space given in Eq. (9). The $\mu-$term is determined by the REWSB condition through its square, but its sign remains undetermined. We assume it to be positive, and accept only solutions which are compatible with the REWSB condition in our scans. Another strong constraint comes from the relic abundance of charged supersymmetric particles [173]. This constraint excludes regions which yield charged particles such as stop and stau to be the LSP. In this context, we require the solutions to yield one of the neutralinos to be the LSP. In this case, it is also desirable that the LSP becomes a suitable dark matter candidate. The thermal relic abundance of LSP should, of course, be consistent with the current results from the WMAP [174] and Planck [175] satellites. However, even if a solution does not satisfy the dark matter observations, it can still survive in conjunction with other form(s) of the dark matter [19,176]. We mostly focus on the LHC allowed solutions, but we also discuss the DM implications in our results.

In addition to these requirements, we also successively apply the mass bounds on the supersymmetric mass spectrum [177] and the constraints from the rare B-decays ($B_s \to \mu^+\mu^-$ [178], $B_s \to X_s\gamma$ [179] and $B_u \to \tau\nu_\tau$ [180]). The rare decays of $B-$meson is calculated by employing Flavorkit [181] interfaced into SPheno. The Standard Model predictions on the processes BR($B_s \to \mu^+\mu^-$) [182] and $B_s \to X_s\gamma$ [183,184] are in a very good agreement with the experimental observations and measurements. Thus, the new physics contributions are expected not to spoil this strong agreement. Even though it is not listed in the experimental constraints, another important impact comes from $K - \bar{K}$ mixing. The Standard Model predictions in $K - \bar{K}$ mixing are strongly approved by the experimental results, and it restricts the solutions such that the first and second family down-type squarks must be almost degenerate ($m_{\tilde{d}} \simeq m_{\tilde{s}}$) [185]. We accept only solutions which do not conflict with this requirement.

In applying the mass bounds, we listed the Higgs boson [1,2] and gluino [86] masses separately, since they have received further updates by the LHC experiments since LEP II. These constraints can be listed as follows:

$$\begin{aligned} & 123 \leq m_h \leq 127 \text{ GeV} \\ & 2100 \text{ GeV} \leq m_{\tilde{g}} \\ & 0.8 \times 10^{-9} \leq BR(B_s \to \mu^+\mu^-) \leq 6.2 \times 10^{-9} \ (2\sigma) \\ & 2.9 \times 10^{-4} \leq BR(b \to s\gamma) \leq 3.87 \times 10^{-4} \ (2\sigma) \\ & 0.15 \leq \frac{BR(B_u \to \nu_\tau\tau)_{MSSM}}{BR(B_u \to \nu_\tau\tau)_{SM}} \leq 2.41 \ (3\sigma) \\ & 0.0913 \leq \Omega h^2(\text{WMAP}) \leq 0.1363 \ (5\sigma) \\ & 0.114 \leq \Omega h^2(\text{Planck}) \leq 0.126 \ (5\sigma). \end{aligned} \tag{10}$$

We allow 2 GeV uncertainty in the Higgs boson mass in order to account the theoretical uncertainties in calculation. The main theoretical uncertainties in the calculation of the Higgs boson result from the uncertainties in the measurements of the top quark mass (m_t) and strong coupling (α_G). Overall uncertainty from m_t and α_G can be as large as about 3 GeV [186]. In addition, the uncertainty in the contributions from the supersymmetric particles can yield about 1.5 (0.5) GeV uncertainty in the case of large (small) stop mixing [187,188]. Thus, the overall uncertainty in the Higgs boson mass calculation can be $2-3$ GeV, and the public spectrum calculators are more or less in agreement in this result [81,189,190]. Spheno employs one-loop RG improved scalar Higgs potential, which is accounted for the two-loop contributions to the Higgs boson mass. Besides, it employs the two-loop matching condition on the quartic Higgs boson coupling between M_{SUSY} and M_Z [191].

In employing the Planck and WMAP bounds on the relic density of the dark matter we set the uncertainty at 5σ to compensate the large theoretical uncertainties in its calculation. Such uncertainties arise from the different handling of the RGEs in the spectrum calculators, assumptions in calculating the gauge and Yukawa couplings etc. [192]. These uncertainties are exponentially enhanced when they are employed in the calculation of the relic density by solving Boltzmann equation. The works on the theoretical uncertainties in relic density calculation revealed that allowing an uncertainty within 5σ can compensate the impact from such theoretical uncertainties [193,194].

In scanning the parameter space we use an interface, which employs the Metropolis-Hasting algorithm described in [195,196]. After generating the low scale data with SPheno, all outputs are transferred to MicrOmegas [197,198] for calculations of the relic abundance of the LSP neutralino as a candidate for DM. The solutions satisfying all the constraints mentioned above (except those from the DM observations) are so-called LHC allowed solutions. Once they are obtained, we transferred their output files from SPheno to

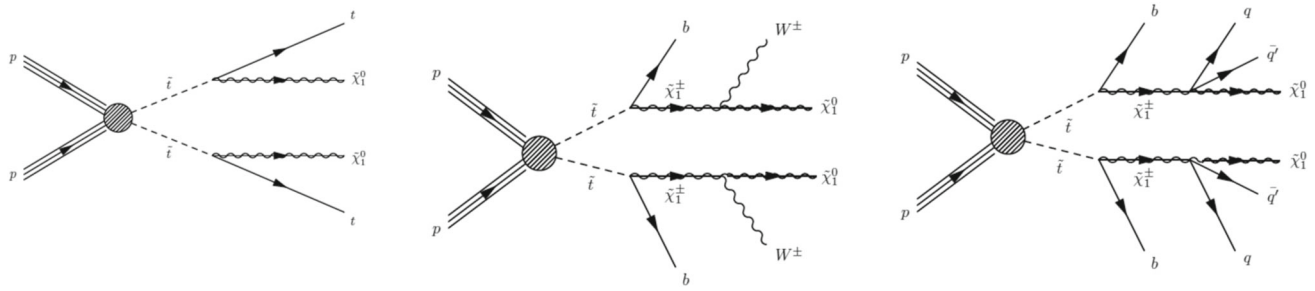

Fig. 1 Topologies for Signal 1 (left), Signal 2 (middle) and Signal 3 (right)

MadGraph [199] for calculation of the cross-sections for the possible signal processes and relevant SM backgrounds. The possible signal processes, whose topologies are illustrated in Fig. 1, can be summarized as follows [89]:

$$\begin{aligned}
&\text{Signal 1: } pp \to \tilde{t}_1\tilde{t}_1 \xrightarrow{\tilde{t}_1 \to t\tilde{\chi}_1^0} t\bar{t}\tilde{\chi}_1^0\tilde{\chi}_1^0 \\
&\text{Signal 2: } pp \to \tilde{t}_1\tilde{t}_1 \xrightarrow{\tilde{t}_1 \to b\tilde{\chi}_1^\pm} b\bar{b}\tilde{\chi}_1^\pm\tilde{\chi}_1^\mp \\
&\qquad\qquad \xrightarrow{\tilde{\chi}_1^\pm \to W^\pm\tilde{\chi}_1^0} b\bar{b}W^\pm W^\mp\tilde{\chi}_1^0\tilde{\chi}_1^0 \\
&\text{Signal 3: } pp \to \tilde{t}_1\tilde{t}_1 \xrightarrow{\tilde{t}_1 \to b\tilde{\chi}_1^\pm} b\bar{b}\tilde{\chi}_1^\pm\tilde{\chi}_1^\mp \\
&\qquad\qquad \xrightarrow{\tilde{\chi}_1^\pm \to q\bar{q}'\tilde{\chi}_1^0} b\bar{b}(q\bar{q}')(q\bar{q}')\tilde{\chi}_1^0\tilde{\chi}_1^0
\end{aligned} \tag{11}$$

The signal processes require the mass difference between the lightest stop and the LSP neutralino to be greater than the mass of a top quark (for Signal 1) or a $W-$boson approximately (for Signal 2). If the stop is not realized to be heavy enough, then the stop may involve in the processes in which it decays into a charm quark along with a LSP neutralino. However, the charm quark signal is overwhelmed by the process $\tilde{t}_1 \to f\bar{f}'b\tilde{\chi}_1^0$ [200], and such a signal cannot provide a clear detection for the stop, and it can probe the stop mass up to about 550 GeV [201]. Even though a similar discussion can be followed for Signal 2, the mass difference between the stop and LSP neutralino is not the only factor, but nature of the stop and the chargino are also important. In the case of Wino-like chargino, the lightest stop should be formed mostly by the superpartner of the left-handed component of the top quark, which, for simplicity, we will refer to as left-handed stop. Hereafter, when we mention the handedness in the name of a supersymmetric scalar particle, it will mean the handedness of its SM partner. On the other hand, if the Higgsino forms the lightest chargino, then the decay mode is open for both left- and right-handed stops. Moreover, the signal is expected to be stronger when Higgsino takes part, since the interaction is proportional to the top quark Yukawa coupling and trilinear scalar interaction term A_t. However, a Higgsino-like chargino leads to another suppression from the $\tilde{\chi}_1^\pm \to W^\pm\tilde{\chi}_1^0$. The chargino-neutralino-W vertex in MSSM can be written as

$$\begin{aligned}
\Gamma_{\tilde{\chi}_1^\pm-\tilde{\chi}_1^0-W_\mu} = &-\frac{i}{2}g_2\left(2U_{11}^*N_{12} + \sqrt{2}U_{12}^*N_{13}\right)\left(\gamma_\mu\frac{1-\gamma_5}{2}\right) \\
&+\frac{i}{2}g_2\left(\sqrt{2}N_{14}^*V_{12} - 2N_{12}^*V_{11}\right)\left(\gamma_\mu\frac{1+\gamma_5}{2}\right)
\end{aligned} \tag{12}$$

where N_{ij} is the matrix encoding the mixing of bino, wino and Higgsinos in forming the neutralino mass eigenstates, while U_{ij} and V_{ij} diagonalize the chargino mass matrix. If the Higgsino dominates in the lightest chargino ($U_{12}(V_{12}) \gg U_{11}(V_{11})$), a strong signal also requires N_{13} and N_{14} to dominate in forming the LSP neutralino. In this case, the Higgsinos form both the LSP neutralino and lightest chargino, and so both are of mass about μ, which kinematically forbids $\tilde{\chi}_1^\pm \to W^\pm\tilde{\chi}_1^0$. Another possibility is that the LSP neutralino can be formed mostly by bino, while the lightest chargino remains higgsino-like. In this case N_{13} and N_{14} will be small, and the signal might not still yield any visible effect. In sum, Signal 2 is available if the lightest stop mass eigenstate is formed mostly by the left-handed stop. However, a similar signal can be realized when the right-handed stop takes part in the processes. In this case, the chargino decay into two quarks along with a LSP neutralino can be considerable, which is shown in the decay cascades of Signal 3.

All the possible signal processes start with the production of a pair of stop quarks; which occurs through $q\bar{q}$ and gg interactions. $q\bar{q}$ interactions can contribute when the stop is light. In both cases, the stop pair production is mediated by the gluon; thus, the cross-section can be calculated by considering the virtual and soft gluon processes, as well as hard gluon processes. While all these processes can contribute either positively or negatively, the processes involving $q\bar{q}$ interactions and/or hard gluon contributions become negligible at the heavy mass scales of the stop. When the stop weighs more than about 1 TeV, the gluon interactions with virtual and soft gluon mediators are expected to be the main channel in the stop pair production (for more details, see [202]).

Since the stop pair production is the trigger in all the signal processes, the pair production of the top quarks forms the most dominant background processes. Nevertheless, its final state is quite similar to the signal processes, and the cuts suppressing the background lead to a significant decrease in the signal cross-section [95]. Before concluding, we should note that the following approximation has been used in calculation of the cross-sections:

$$\begin{aligned}
&\sigma(\text{Signal 1}) \approx \sigma(pp \to \tilde{t}_1\tilde{t}_1) \times \text{BR}(\tilde{t}_1 \to t\tilde{\chi}_1^0)^2 \\
&\sigma(\text{Signal 2}) \approx \sigma(pp \to \tilde{t}_1\tilde{t}_1) \times \text{BR}(\tilde{t}_1 \to b\tilde{\chi}_1^\pm)^2 \\
&\quad \times \text{BR}(\tilde{\chi}_1^\pm \to W^\pm\tilde{\chi}_1^0)^2 \\
&\sigma(\text{Signal 3}) \approx \sigma(pp \to \tilde{t}_1\tilde{t}_1) \times \text{BR}(\tilde{t}_1 \to b\tilde{\chi}_1^\pm)^2 \\
&\quad \times \text{BR}(\tilde{\chi}_1^\pm \to q\bar{q}'\tilde{\chi}_1^0)^2
\end{aligned} \tag{13}$$

where the production cross-section of a pair of stop quarks are calculated by MadGraph, while the branching ratios are used from SPheno. The full matrix element calculation has been performed over a control group, and the approximation given in Eq. (13) yields only about 0.7% error in comparison to the full calculation [87]. The signal strength (SS) over the background processes is quantified as

$$SS = \frac{S}{\sqrt{S+B}}, \tag{14}$$

where S and B refer to the event numbers (cross-section $\times$ Luminosity) of the signal and background respectively. We use the following correspondence to translate SS to the confidence level (CL) [203]:

$$\begin{aligned}
&0 \le SS < 1 \to \text{hardly probed (Blue)}, \\
&1 \le SS < 2 \to \text{probed up to 68\% (Red)}, \\
&2 \le SS < 3 \to \text{probed up to 95\% (Black)} \\
&SS > 3 \qquad\quad \to \text{discovery (Green)},
\end{aligned} \tag{15}$$

where we identify the solutions with $SS > 3$ to be the prediction of a discovery in this class of SO(10) GUT models. The intervals of the signal strength will be shown in plots with colors as given in the parentheses, when we discuss the signals and the impacts from the current and future collider experiments in Sect. 5.

4 Mass spectrum and signal profile

In this section we discuss the mass spectrum of supersymmetric particles with the emphasis on those, which participate in possible stop signals, and consider if the signal processes summarized in the previous section are available. Figure 2 displays first the gluino and LSP neutralino masses in comparison to the stop mass with plots in the $m_{\tilde{g}} - m_{\tilde{t}_1}$ and $m_{\tilde{t}_1} - m_{\tilde{\chi}_1^0}$ planes. The stop can be as heavy as about 8 TeV, while the gluino mass can go up to about 10 TeV and beyond, as seen in the $m_{\tilde{g}} - m_{\tilde{t}_1}$ plane. We did not show the region where $m_{\tilde{g}} > 10$ TeV, since it is beyond the reach of the current and future collider experiments, even after a high luminosity is achieved [87]. The results also reveal that the region with gluino lighter than stop (below the diagonal line in the $m_{\tilde{g}} - m_{\tilde{t}_1}$ plane) is mostly excluded by the current bound on the gluino mass, and only a small portion of the parameter space can kinematically allow the $\tilde{t} \to \tilde{g}t$ process, which may not provide enough statistics to probe the stop through this channel. On the other hand, the $m_{\tilde{t}_1} - m_{\tilde{\chi}_1^0}$ plane shows that most of the solutions can yield enough mass difference between the stop and LSP neutralino that the $\tilde{t}_1 \to t\tilde{\chi}_1^0$ process is allowed. As can be seen, the LSP neutralino mass can lie from about 0.2 to 2.3 TeV, while the stop mass can be realized as heavy as about 8 TeV. In addition, the diagonal line indicates the mass degeneracy between the stop and LSP neutralino, and the solutions around it allow only $\tilde{t} \to c\tilde{\chi}_1^0$.

We display our results in Fig. 3 with plots in the $m_{\tilde{t}_1} - m_{\tilde{\chi}_1^\pm}$ and $m_{\tilde{t}_L} - m_{\tilde{t}_R}$ planes. The color coding is the same as in Fig. 2. The $m_{\tilde{t}_1} - m_{\tilde{\chi}_1^\pm}$ plane shows that the chargino can be realized as heavy as 3 TeV, while the DM constraints bound its mass at about 2.7 TeV. Comparing the masses of stop and chargino the stop seems to be able to decay into a chargino in most of the parameter space, while it is kinematically forbidden only in a small portion (below the diagonal line). However, the LHC allowed region yield the left-handed stop to be heavier than the right-handed state at all. The solutions around the diagonal line predict $m_{\tilde{t}_L} \simeq m_{\tilde{t}_R}$. In this case, the left-handed stop can provide some contributions to the nature of the lightest chargino through its mixing with the right-handed stop. As is discussed in the previous section, when the lightest stop mass state is formed mostly by the right-handed stop, the processes involving $W^\pm$−boson, as in Signal 2, rather yield weak signal strengths, and one may not probe the stop through such events. Recall that Signal 3 can still be available, when the right-handed stop happens to be lighter than the left-handed stop.

In addition to the stop, Fig. 4 discusses the nature of the chargino and LSP neutralino with plots in the $M_2 - \mu$ and $M_1 - \mu$ planes. The color coding is the same as in Fig. 2. M_1 and M_2 represent the bino and wino masses at the SUSY scale, while μ stands for the Higgsino mass. As seen from the $M_2 - \mu$ plane, Higgsino is realized heavier than wino over most of the parameter space. In this case, the lightest chargino is mostly formed by wino, which yields a weak signal strength for the $\tilde{t}_1 \to b\tilde{\chi}_1^\pm$. However, there is a region above the diagonal line, in which the Higgsino happens to be lighter and forms the lightest chargino. In this case, even though $\text{BR}(\tilde{t}_1 \to b\tilde{\chi}_1^\pm)$ can be large, Signal 2 is strongly suppressed since $m_{\tilde{\chi}_1^\pm} \sim m_{\tilde{\chi}_1^0} \sim \mu$ and $\text{BR}(\tilde{\chi}_1^\pm \to W^\pm\tilde{\chi}_1^0) \sim 0$. However, the processes of Signal 2 can be made available by replacing $\tilde{\chi}_1^\pm \to W^\pm\tilde{\chi}_1^0$ with

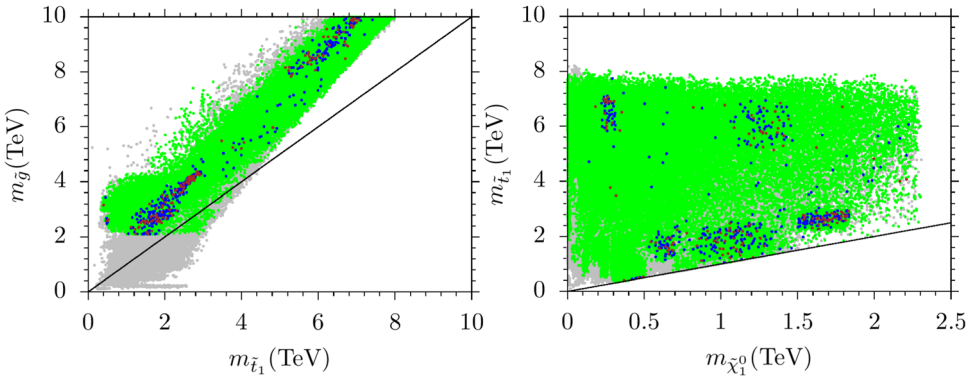

Fig. 2 Plots in the $m_{\tilde{g}} - m_{\tilde{t}_1}$ and $m_{\tilde{t}_1} - m_{\tilde{\chi}_1^0}$ planes. All points are compatible with the REWSB and LSP neutralino conditions. Green points satisfy the mass bounds and the constraints from rare $B-$meson decays. Blue and brown points form subsets of green, and they are allowed by the constraints on the relic abundance of LSP neutralino set by the WMAP and Planck satellites, respectively. The diagonal lines indicate the mass degeneracy between the displayed particles

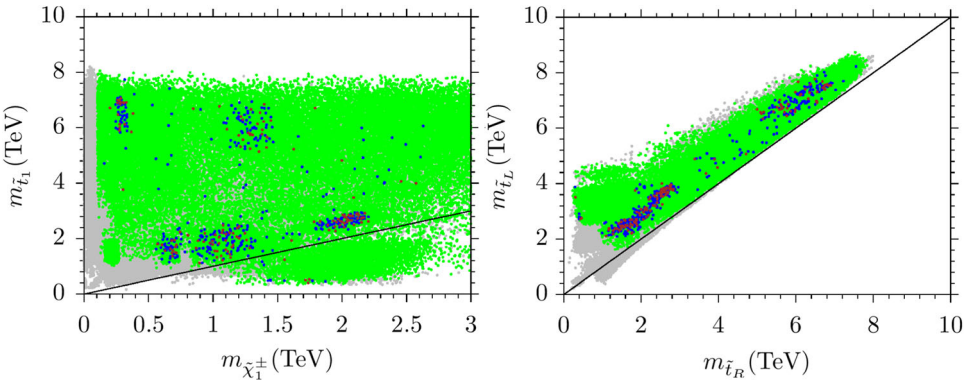

Fig. 3 Plots in the $m_{\tilde{t}_1} - m_{\tilde{\chi}_1^\pm}$ and $m_{\tilde{t}_L} - m_{\tilde{t}_R}$ planes. The color coding is the same as in Fig. 2

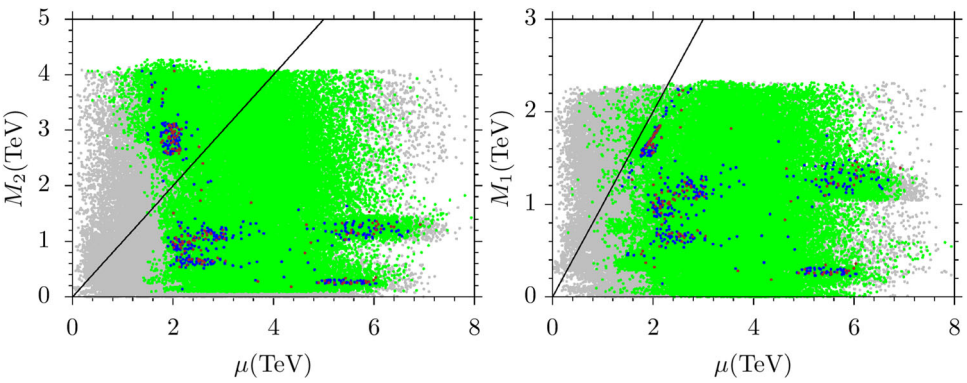

Fig. 4 Plots in the $M_2 - \mu$ and $M_1 - \mu$ planes. The color coding is the same as in Fig. 2

$\tilde{\chi}_1^\pm \to q\bar{q}'\tilde{\chi}_1^0$, as is classified in Signal 3. The $M_1 - \mu$ plane shows that bino is mostly lighter than Higgsino, and comparing two panels of Fig. 4 reveals that the lightest neutralino is formed mostly by bino or bino-wino mixture, though bino-higgsino mixture is also available.

5 Probing stop in collider experiments

In the previous section, we discussed the available signal processes in terms of masses and flavors of the relevant particles, and concluded that $\tilde{t}_1 \to t\tilde{\chi}_1^0$ and the $\tilde{t}_1 \to b\tilde{\chi}_1^\pm \to bq\bar{q}'\tilde{\chi}_1^0$ decay modes are likely to provide most promising signals in this class of SUSY GUTs. However, even though we select

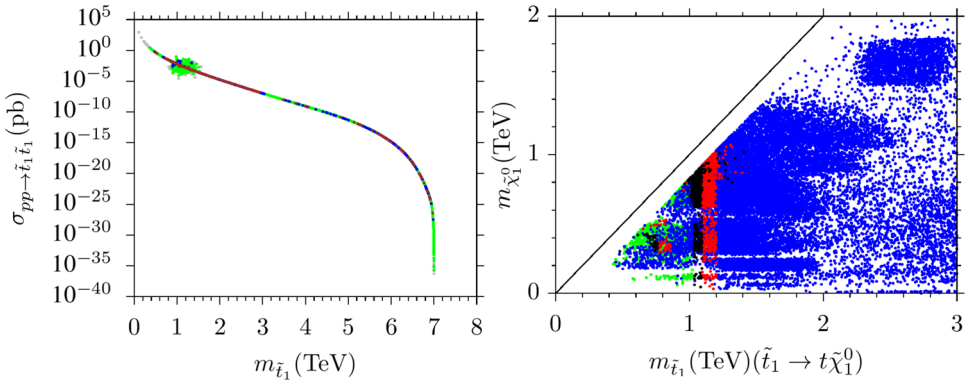

Fig. 5 Plots for the stop pair production and LSP neutralino-stop mass correlation in the $\sigma(pp \to \tilde{t}_1\tilde{t}_1) - m_{\tilde{t}_1}$ and $m_{\tilde{\chi}_1^0} - m_{\tilde{t}_1}$ planes. The color coding in the left panel is the same as in Fig. 2. In the right panel, all solutions satisfy the mass bounds and the constraints from rare $B-$meson decays. Blue points represent the solutions with $SS(\text{Signal 1}) < 1$, while red, black and green correspond to $1 \leq SS(\text{Signal 1}) < 2$, $2 \leq SS(\text{Signal 1}) < 3$ and $SS(\text{Signal 1}) \geq 3$, respectively for 14 TeV with 36.1 fb^{-1} luminosity

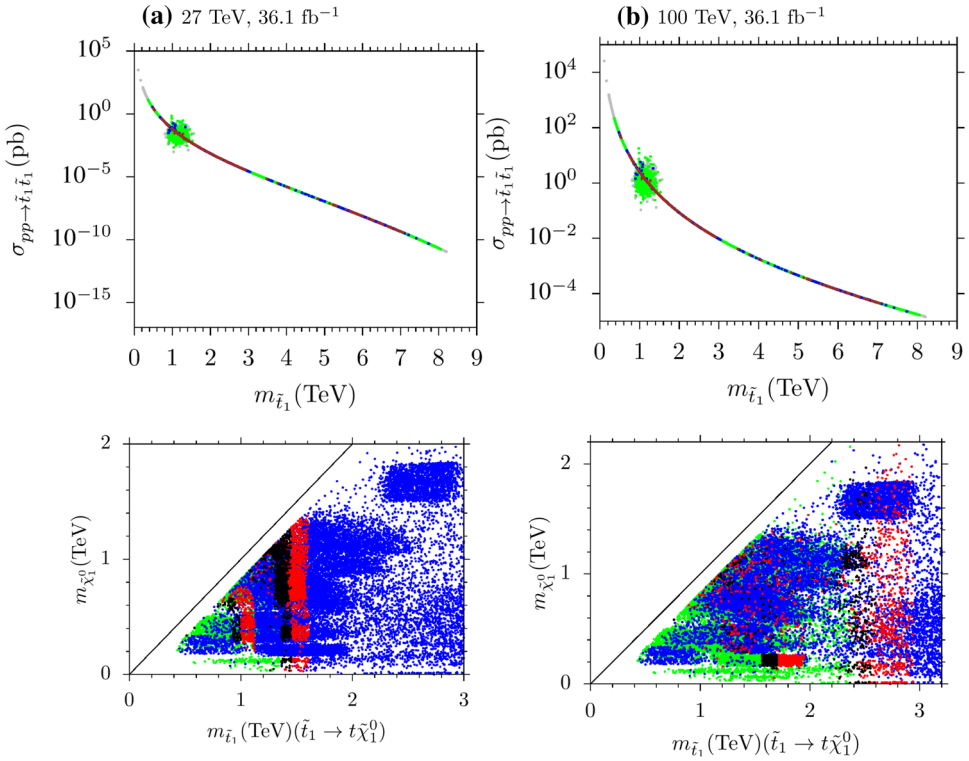

Fig. 6 Plots for the stop pair production and LSP neutralino-stop mass correlation in the $\sigma(pp \to \tilde{t}_1\tilde{t}_1) - m_{\tilde{t}_1}$ and $m_{\tilde{\chi}_1^0} - m_{\tilde{t}_1}$ planes at 27 TeV (left) and 100 TeV (right) center of mass energies. The color coding is the same as in Fig. 5

the most optimized benchmark points which yield the largest branching ratios in the processes listed in Eq. (11), the main suppression comes from the smallness of the stop pair production cross-section. Figure 5 represents the cross-section for the stop pair production and the strength of the processes classified in Signal 1. The $\sigma(pp \to \tilde{t}_1\tilde{t}_1) - m_{\tilde{t}_1}$ plane shows that the stop pair in the LHC allowed region (green) can be produced at $\sigma(pp \to \tilde{t}_1\tilde{t}_1) \sim 1$ pb when the stop weighs about 500 GeV, and it drops below 10^{-5} pb for $m_{\tilde{t}_1} \gtrsim 2$ TeV. Even though the correlation between the cross-section of the stop pair production and the stop mass is mostly a smooth curve, there is a region of scattered points. This region happens as a result of an interplay among the different processes of stop pair production such as $q\bar{q}$ interactions and hard gluon corrections, as mentioned before. Following the approximation given in Eq. (13) and assuming absence of a direct signal, the $m_{\tilde{\chi}_1^0} - m_{\tilde{t}_1}$ plane shows that the results can exclude the stop masses up to about 1.2 TeV at 68% CL (red), while

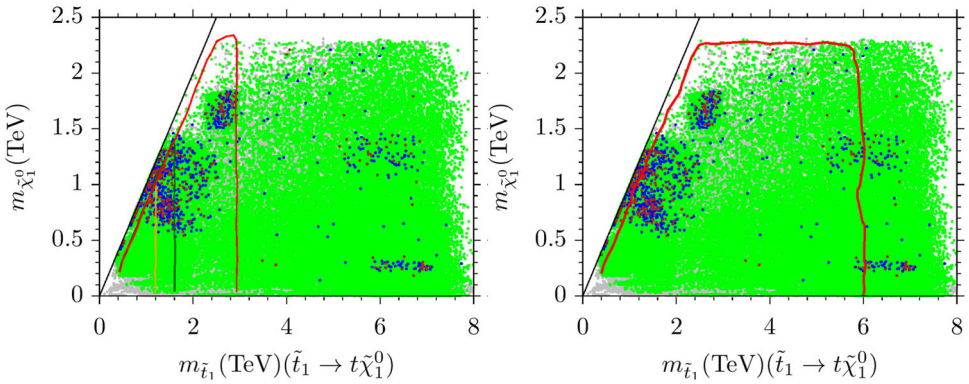

Fig. 7 Exclusion curves for the stop mass through $\tilde{t}_1 \to t\tilde{\chi}_1^0$. The color coding is the same as in Fig. 2. In the left panel, orange curve represents the exclusion at the current energy, while the dark green and red are obtained at 27 TeV and 100 TeV, repsectively. Luminosity is set to 36.1 fb^{-1} at all energies. The right panel is the same exclusion curve for the stop mass at 100 TeV center of mass energy and 3000 fb^{-1} luminosity

$m_{\tilde{t}_1} \lesssim 1.1$ TeV is excluded at 95% CL (black). Note that the blue points represent the solutions with $SS < 1$, which means the stop does negligibly decay into a LSP neutralino along with a top quark. Thus, our analyses and results do not apply to the solutions shown in blue.

We continue to discuss the stop pair production and the strength of Signal 1 in Fig. 6 with plots in the $\sigma(pp \to \tilde{t}_1\tilde{t}_1) - m_{\tilde{t}_1}$ and $m_{\tilde{\chi}_1^0} - m_{\tilde{t}_1}$ planes at 27 TeV (left) and 100 TeV (right) center of mass energies. The color coding is the same as in Fig. 5. The luminosity is set to 36.1 fb^{-1} in both cases. When the center of mass energy is raised to 27 TeV, the stop pair production cross-section is realized of the order $\mathcal{O}(10)$ pb, while it can be expected as high as $\mathcal{O}(100)$ pb in the collider experiments with 100 TeV center of mass energy, as seen from the top panels. The strength of Signal 1 should be enhanced accordingly. The bottom panel shows that the stop can be probed to about 1.6 TeV at 27 TeV, and about 3 TeV at 100 TeV with 68% CL (red). Requiring 95% CL yield the mass scales of about 1.4 TeV at 27 TeV, and 2.6 TeV at 100 TeV (black) to probe the stop, if the stop decays follow the cascade in Signal 1.

Figure 7 summarizes our finding in the analyses over Signal 1 in the $m_{\tilde{\chi}_1^0} - m_{\tilde{t}_1}$ plane. The color coding is the same as in Fig. 2. In the left panel, orange curve represents the exclusion at the current energy, while the dark green and red are obtained at 27 TeV and 100 TeV, respectively. Luminosity is set to 36.1 fb^{-1} at all energies. The right panel is the exclusion curve for the stop mass at 100 TeV center of mass energy and 3000 fb^{-1} luminosity. As seen from the left panel, the current collider experiments can exclude the stop within the mass scales up to about 1.2 TeV, while the future experiments with 27 TeV and 100 TeV center of mass energy are promising to probe the stop up to about 1.6 TeV and 3 TeV, respectively. The right panel displays the reachable mass scales when 3000 fb^{-1} luminosity is achieved at 100 TeV. As seen from the results, the stop will be able to be probed up to about 6 TeV, if it decays into a LSP neutralino along with a top quark.

As we discussed in the previous section, Signal 2 is not expected to be strong enough due to the right-handed stop forming the lightest stop mass eigenstate, unless the left handed-stop can take part considerably in forming $\tilde{t}_1$. A sizeable mixing between left- and right-handed stops requires large A_t and/or $\tan\beta$. However, avoiding a color/charge breaking minimum requires $A_t^2 < 3(m_{\tilde{t}_R}^2 + m_{\tilde{t}_L}^2 + m_{H_u}^2)$ [204], which may result in heavier stop at the weak scale, and such solutions could be beyond the reach of the current collider experiments. The impact of mixing between the left- and right-handed stops is shown in Fig. 8 with plots in the $m_{\tilde{\chi}_1^0} - m_{\tilde{t}_1}$ plane at 14 TeV with 36.1 fb^{-1} luminosity (left), and 100 TeV with 3000 fb^{-1} luminosity (right). The green, black and red points indicate that Signal 2 can be available only if the solutions lead to $0.8 \lesssim m_{\tilde{t}_1} \lesssim 1.2$ TeV and $0.6 \lesssim m_{\tilde{\chi}_1^0} \lesssim 1$ TeV. On the other hand, the right panel displays interesting results that Signal 2 becomes available for the analyses when 3000 fb^{-1} luminosity is reached at 100 TeV collider experiments. Indeed, one can probe the stop mass up to about 4.8 TeV through Signal 2 in the future experiments. As discussed before, the processes represented as Signal 2 are available when the Wino significantly contributes to the composition of the chargino, and the LSP neutralino is mostly Bino-like. In this case, the Signal 2 processes can occur through the mixing of the left-handed stop in $\tilde{t}_1$ because of the chirality of $SU(2)_L$. In this context, the future results can also probe the mixing between the left- and right-handed stops in this class of $SO(10)$ GUT models.

Finally, we discuss the results for Signal 3 from similar analyses performed for Signal 1 and Signal 2 in Fig. 9 by displaying the exclusion curves at various center of mass energies. The left panel shows that the current experiments can exclude the stop mass below about 1.2 TeV, while it can be probed up to about 2 TeV at 27 TeV and 2.8 TeV at 100

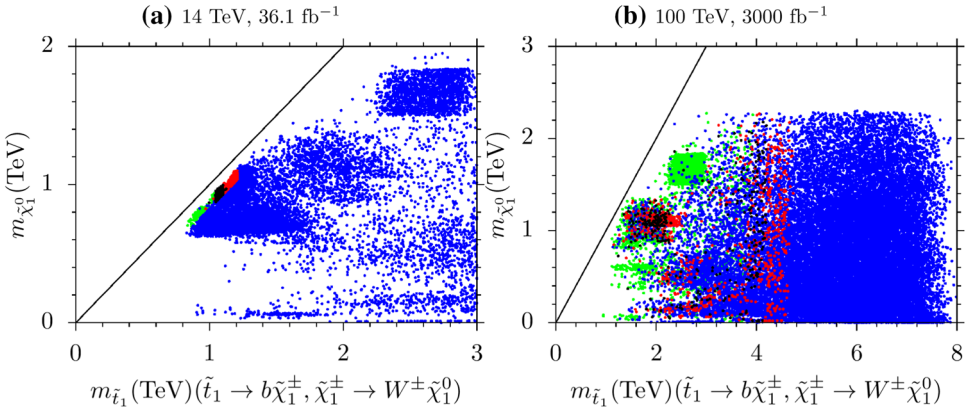

Fig. 8 Plots in the $m_{\tilde{\chi}_1^0} - m_{\tilde{t}_1}$ plane at 14 TeV with 36.1 fb^{-1} luminosity (left), and 100 TeV with 3000 fb^{-1} luminosity (right). All solutions satisfy the mass bounds and the constraints from rare $B-$meson decays. Blue points represent the solutions with $SS(\text{Signal 2}) < 1$, while red and black correspond to $1 \leq SS(\text{Signal 2}) \leq 2$, and $2 \leq SS(\text{Signal 2}) \leq 3$, respectively. The green points yield $SS > 3$

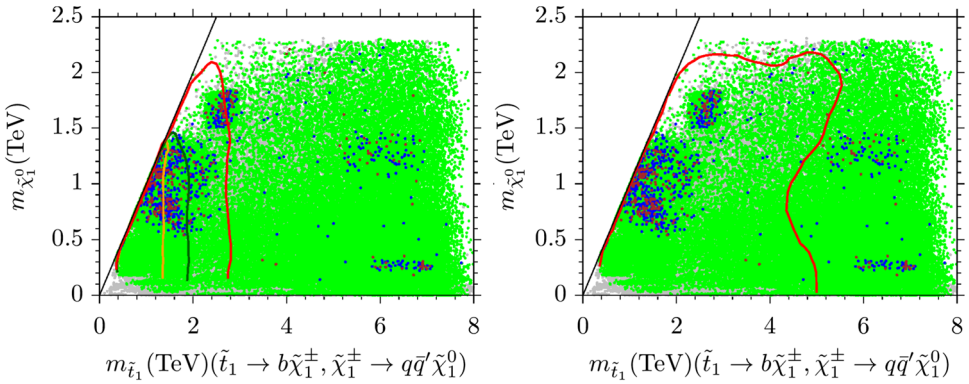

Fig. 9 Exclusion curves for the stop mass through $\tilde{t}_1 \to b\tilde{\chi}_1^\pm$ with $\tilde{\chi}_1^\pm \to q\bar{q}'\tilde{\chi}_1^0$. The color coding is the same as in Fig. 2. In the left panel, orange represents the exclusion at the current energy, while the dark green and red are obtained at 27 TeV and 100 TeV, repsectively. Luminosity is set to 36.1 fb^{-1} at all energies. The right panel is the same exclusion curve for the stop mass at 100 TeV center of mass energy and 3000 fb^{-1} luminosity

TeV. The right panel reveals that the future experiments can probe the stop masses further up to about 5 TeV through Signal 3, if Signal 3 is available.

Finally, we exemplify our findings for the signal processes over three tables of benchmark points. We select these benchmark points such that they are all allowed by the current mass bounds and the constraints from rare $B-$meson decays. We employ the bound on the relic density of LSP neutralino when there exists a solution for the 68% and 95% CL probes of stop. Table 1 displays four benchmark points, which can be tested in the current and future collider experiments through the Signal 1 processes. Point 1 predicts a signal strength of 1.12 in the collisions with 14 TeV center of mass energy and 36.1 fb^{-1} luminosity, which corresponds to 68% CL exclusion. Point 2 shows a solution which can be probed at 68% CL in the collision experiments with 27 TeV center of mass energy. Point 3 depicts a solution which can be probed at 95% CL, when the center of mass energy of the collisions is set to 100 TeV. Even though the mass spectrum is heavier than those shown in Points 1 and 2, the pair production cross-section of stops will be expected to be high in these collision experiments. Point 4 displays a solution for 68% CL probe of the stop when 3000 fb^{-1} luminosity is reached in the collisions with 100 TeV center of mass energy. The stop mass in such solutions is about 5.8 TeV, and its pair production cross-section is expected to be small in comparison with the other points in Table 1. Point 4 shows that future collider experiments with high center of mass energy and high luminosity will have the sensitivity to probe such solutions. In all these points, the LSP neutralino is formed mostly by Bino, while Wino mass is also near by the Bino mass. Higgsinos do not take part in forming LSP neutralino, since their masses are as $\mu \sim m_0$. Considering small branching ratios for the $\tilde{t} \to b\tilde{\chi}_1^\pm$ processes, these points cannot be tested through the processes given in Signal 2 and Signal 3, and thus, they

Table 1 Benchmark points for Signal 1 which can be tested in the current and near future experiments within 68% and 95% CL. All masses are given in GeV unit, while the units of other parameters are given in the table. All points are chosed as to be consistent with the mass bounds and rare $B-$ meson decays. The constraint on the relic density of LSP neutralino is applied when there exist a solution within 68% and/or 95% CL probe

Signal 1	Point 1	Point 2	Point 3	Point 4
m_0	2120	3232	2859	4060
M_1	1974	1467	2377	2827
M_2	1069	799.3	1285	1542
M_3	1028	1063	1306	4142
$\tan\beta$	17.7	27.7	1.65	21.5
A_0/m_0	-2.35	-2.05	-1.26	-1.93
μ	2398	2792	2077	5550
m_h	124.1	125.3	123.6	126.5
m_H	3028	3489	3453	6390
m_A	3028	3488	3452	6389
$m_{H^\pm}$	3029	3490	3453	6389
$m_{\tilde{g}}$	2355	2488	2957	8418
$m_{\tilde{u}_{1,2}}$	2879, 2912	3767, 3777	3735, 3772	8083, 8097
$m_{\tilde{d}_{1,2}}$	2851, 2913	3757, 3777	3705, 3773	8068, 8098
$m_{\tilde{t}_{1,2}}$	1121, 2174	1483, 2627	2309, 3098	5785, 6879
$m_{\tilde{b}_{1,2}}$	2148, 2709	2606, 3334	3084, 3602	6870, 7783
$m_{\tilde{e}_{1,2}}$	2238, 2248	3271, 3274	2987, 2994	4179, 4188
$m_{\tilde{\tau}_{1,2}}$	2049, 2162	2709, 3007	2867, 2938	3782, 3988
$m_{\tilde{\chi}^0_{1,2}}$	872.7, 894.8	653, 682	1058, 1077	1274, 1290
$m_{\tilde{\chi}^0_{3,4}}$	2392, 2393	2785, 2786	2108, 2111	5612, 5612
$m_{\tilde{\chi}^\pm_{1,2}}$	894.9, 2394	682.1, 2787	1077, 2111	1289, 5613
$\mathrm{BR}(\mathrm{B_s}\to\mu\mu)$	3.2×10^{-9}	3.3×10^{-9}	3.2×10^{-9}	3.23×10^{-9}
$\mathrm{BR}(B\to X_s\gamma)$	3.06×10^{-4}	3.04×10^{-4}	3.13×10^{-4}	3.15×10^{-4}
Ωh^2	0.120	0.122	0.121	0.120
σ^{SI} (pb)	2.87×10^{-9}	1.21×10^{-9}	1.75×10^{-8}	7.92×10^{-11}
σ^{SD} (pb)	5.38×10^{-9}	2.02×10^{-9}	1.73×10^{-8}	1.19×10^{-10}
$\mathrm{BR}(\tilde{t}_1\to t\tilde{\chi}^0_1)$	0.81	0.90	0.65	0.93
$\mathrm{BR}(\tilde{t}_1\to b\tilde{\chi}^\pm_1)$	0.13	0.07	0.15	0.03
$\mathrm{BR}(\tilde{\chi}^\pm_1\to W\tilde{\chi}^0_1)$	–	–	–	–
$\mathrm{BR}(\tilde{\chi}^\pm_1\to qq'\tilde{\chi}^0_1)$	0.69	0.43	0.42	0.78
$\sigma(pp\to\tilde{t}\tilde{t})$ (pb)	2.67×10^{-3}	5.48×10^{-3}	3.98×10^{-2}	1.75×10^{-4}
SS	1.12	1.40	2.69	1.17
$\sqrt{s}$ (TeV)	14	27	100	100
$\mathcal{L}$ (fb^{-1})	36.1	36.1	36.1	3000

are included in regions of blue points in the plots discussed for Signal 2 and Signal 3.

Table 2 represents two benchmark points which can be tested in the current and future experiments at 95% CL or beyond. In these solutions, the left- and right-handed stops mix considerably in forming the lightest mass eigenstate of stop such that its decay into the lightest chargino along with a bottom quark has large enough to be probed. Point 1 displays a solution in which $\mathrm{BR}(\tilde{t}_1\to b\tilde{\chi}^\pm_1)=\mathrm{BR}(\tilde{\chi}^\pm_1\to W\tilde{\chi}^0_1)=0.99$. This point can be probed only through the Signal 2 processes, and it is in blue region in the plots of Signal 1 and Signal 3. It should also be noted that its signal strength is very high ($SS=42$), and definitely it would have been seen in the current experiments, if there was a direct signal. Point 2 shows a solution which can be probed at 95% CL in the experiments with high center of mass energy and luminosity. Since the chargino decays only into a W boson and LSP neutralino, this point cannot be probed through the other signal processes.

We list four benchmark points also for Signal 3 in Table 3. Point 1 depicts a solution in which the stop decays only into a bottom quark and chargino, and subsequently the chargino decays only into a pair of quarks and LSP neutralino. This solution predicts the signal strength as 2.36 in

Table 2 Benchmark points for 68% and 95% CL probe of stops through Signal 2. Point selection is the same as explained in Table 1

Signal 2	Point 1	Point 2
m_0	2180	3629
M_1	2705	4764
M_2	1546	3327
M_3	849.7	2448
$\tan\beta$	13.6	29.3
A_0/m_0	-1.65	-0.77
μ	1769	2518
m_h	123.1	124.2
m_H	2888	4156
m_A	2888	4154
$m_{H^\pm}$	2889	4155
$m_{\tilde{g}}$	2113	5209
$m_{\tilde{u}_{1,2}}$	2754, 2843	5668, 5908
$m_{\tilde{d}_{1,2}}$	2697, 2843	5586, 5909
$m_{\tilde{t}_{1,2}}$	1216, 2244	3996, 5001
$m_{\tilde{b}_{1,2}}$	2225, 2624	4992, 5231
$m_{\tilde{e}_{1,2}}$	2395, 2435	4024, 4258
$m_{\tilde{\tau}_{1,2}}$	2312, 2394	3588, 4023
$m_{\tilde{\chi}^0_{1,2}}$	1200, 1284	2166, 2575
$m_{\tilde{\chi}^0_{3,4}}$	1772, 1779	2589, 2799
$m_{\tilde{\chi}^\pm_{1,2}}$	1284, 1779	2573, 2798
$\mathrm{BR}(\mathrm{B_s}\to\mu\mu)$	3.23×10^{-9}	3.24×10^{-9}
$\mathrm{BR}(B\to X_s\gamma)$	3.08×10^{-4}	3.14×10^{-4}
Ωh^2	0.58	0.123
σ^{SI} (pb)	4.95×10^{-8}	3.77×10^{-8}
σ^{SD} (pb)	5.16×10^{-8}	3.13×10^{-8}
$\mathrm{BR}(\tilde{t}_1\to t\tilde{\chi}^0_1)$	–	0.12
$\mathrm{BR}(\tilde{t}_1\to b\tilde{\chi}^\pm_1)$	0.99	0.42
$\mathrm{BR}(\tilde{\chi}^\pm_1\to W\tilde{\chi}^0_1)$	0.99	0.99
$\mathrm{BR}(\tilde{\chi}^\pm_1\to qq'\tilde{\chi}^0_1)$	–	–
$\sigma(pp\to\tilde{t}\tilde{t})$ (pb)	1.17×10^{-2}	1.81×10^{-3}
SS	42	2.46
$\sqrt{s}$ (TeV)	14	100
$\mathcal{L}$ (fb^{-1})	36.1	3000

the current experiment, and its exclusion is at 95% CL. Point 2 is listed for the experiments conducted at 27 TeV center of mass energy, which can probe this solution at 95% CL. Point 3 and Point 4 show solutions which can be tested with 100 TeV collisions at 68% and 95% CL, respectively. Point 4 also shows that the future experiments will be so sensitive that the Signal 3 processes can be probed even when $\mathrm{BR}(\tilde{t}_1\to b\tilde{\chi}^\pm_1)\sim 0.06$. The last three points can be also tested through the Signal 1 processes, since they have considerable percentage for the decay $\tilde{t}_1\to t\tilde{\chi}^0_1$.

As seen from the tables of benchmark points, different solutions can yield different observation mechanisms such that a solution can be invisible in one signal process, while it might be strong enough to be probed through another process. In this context, one can conclude the impact from the collider experiments on the stop detection by considering the combined signal strength from all three classes of signals, whose results are shown in Fig. 10. The top left panel displays the total signal strength of stop signals in the collider experiments with 14 TeV center of mass energy, and our results show that all the solutions in the region with $m_{\tilde{t}_1}\lesssim 1.2$ TeV lead to $SS>1$. Following the color coding summarized in Eq. (15) the current experiments can exclude the region with $m_{\tilde{t}}\lesssim 1$ TeV (green), while they can probe the stop mass up to about 1.1 TeV at 95% C.L, and 1.2 TeV at 68% C.L. Despite the blue points, it is also possible to probe the stop mass up to about 1.4 TeV if at least one of these signal processes yield visible strength in the current collider experiments. The top right panel shows the similar results for the 27 TeV center of mass energy. These experiments can probe the stop mass through the signal processes up to about 1.4 TeV. Note that there are a few solutions in this region shown in blue. These solutions predict Wino to be lighter than Bino, and thus the lightest chargino and LSP neutralino are mostly formed by Wino. The right-handedness of the lightest stop suppresses the signal strength for these solutions. Apart from the handedness, it is also possible to probe the stop up to about 1.9 TeV in these experiments.

The bottom panels reveal the results for the 100 TeV collider experiments with 36.1 fb^{-1} (left) and 3000 fb^{-1} (right) luminosity. The 100 TeV collider experiments are expected to probe the solutions for Wino-like LSP discussed for the 27 TeV center of mass energy above, since they provide enough sensitivity to even a small mixing between left- and right-handed stops. In addition, the region with $m_{\tilde{t}_1}\lesssim 2$ TeV is expected to be significantly probe in such experiments. It will also be possible to probe the stop mass up to about 3 TeV, if one of the signals yield enough strength. The probed mass scale for the stop will be shifted about 1–2 TeV when a high luminosity such 3000 fb^{-1} is obtained as shown in the bottom right panel. It is interesting to see the blue points in the region with $2\lesssim m_{\tilde{t}_1}\lesssim 3$ TeV, despite the high luminosity. The gluino can happen to be lighter than stop in this region, and these solutions remain in blue, since we do not consider the signal processes in which the stop decays into a gluino along with a top quark. These solutions are shown in the $m_{\tilde{g}}-m_{\tilde{t}_1}$ plane of Figure 1 (those below the diagonal line). Such signals can be allowed only in a small region, but one can also follow analyses over some benchmark points to explore the sensitivity of the experiments to the $\tilde{t}\to\tilde{g}t$.

In the benchmark points displayed above, the LSP neutralino is mostly bino, while the chargino happens to be NLSP except those listed in Table 2. In this case masses of

Table 3 Benchmark points of stop probes within 68% and 95% CL through Signal 3. The point selection is the same as explained in Table 1

Signal 3	Point 1	Point 2	Point 3	Point 4
m_0	2158	2910	2274	2859
M_1	2786	3515	2518	2377
M_2	1470	1257	1354	1285
M_3	1032	925.3	1137	1306
$\tan\beta$	12.8	30.6	17.5	16.5
A_0/m_0	-2.09	-1.67	-2.14	-1.23
μ	2246	2130	2427	2077
m_h	124	125.1	124.5	124
m_H	3165	2906	3207	3453
m_A	3165	2905	3207	3452
$m_{H^\pm}$	3166	2907	3208	3453
$m_{\tilde{g}}$	2365	2183	2583	2957
$m_{\tilde{u}_{1,2}}$	2944, 3006	3438, 3455	3135, 3185	3735, 3772
$m_{\tilde{d}_{1,2}}$	2887, 3006	3377, 3439	3093, 3185	3705, 3773
$m_{\tilde{t}_{1,2}}$	1294, 2337	1682, 2457	1431, 2444	2309, 3098
$m_{\tilde{b}_{1,2}}$	2315, 2814	2435, 2958	2421, 2953	3084, 3602
$m_{\tilde{e}_{1,2}}$	2387, 2399	3076, 3181	2453, 2467	2987, 2994
$m_{\tilde{\tau}_{1,2}}$	2297, 2360	2654, 2821	2273, 2384	2867, 2938
$m_{\tilde{\chi}^0_{1,2}}$	1226, 1238	1062, 1570	1119, 1133	1058, 1077
$m_{\tilde{\chi}^0_{3,4}}$	2244, 2248	2137, 2140	2425, 2427	2108, 2111
$m_{\tilde{\chi}^\pm_{1,2}}$	1226, 2248	1062, 2140	1132, 2428	1077, 2111
$\mathrm{BR}(\mathrm{B_s} \to \mu\mu)$	3.23×10^{-9}	3.31×10^{-9}	3.24×10^{-9}	3.23×10^{-9}
$\mathrm{BR}(B \to X_s\gamma)$	3.10×10^{-4}	3.02×10^{-4}	3.08×10^{-4}	3.13×10^{-4}
Ωh^2	0.074	0.033	0.121	0.121
σ^{SI} (pb)	1.24×10^{-7}	1.04×10^{-7}	6.90×10^{-9}	1.75×10^{-8}
σ^{SD} (pb)	1.49×10^{-7}	1.14×10^{-7}	9.26×10^{-9}	1.73×10^{-8}
$\mathrm{BR}(\tilde{t}_1 \to t\tilde{\chi}^0_1)$	–	0.31	0.80	0.65
$\mathrm{BR}(\tilde{t}_1 \to b\tilde{\chi}^\pm_1)$	1.00	0.68	0.12	0.06
$\mathrm{BR}(\tilde{\chi}^\pm_1 \to W\tilde{\chi}^0_1)$	–	–	–	–
$\mathrm{BR}(\tilde{\chi}^\pm_1 \to qq'\tilde{\chi}^0_1)$	1.00	0.73	0.78	0.78
$\sigma(pp \to \tilde{t}\tilde{t})$ (pb)	8.87×10^{-4}	2.36×10^{-3}	4.59×10^{-1}	3.98×10^{-2}
SS	2.36	2.48	1.07	2.54
$\sqrt{s}$ (TeV)	14	27	100	100
$\mathcal{L}$ (fb^{-1})	36.1	36.1	36.1	3000

the two lightest neutralinos and lightest chargino are at the same order in the mass spectrum, and the relic density of the LSP neutralino is reduced through the chargino-neutralino coannihilation processes, which result in $\Omega h^2 \simeq 0.12$ for some of the solutions. On the other hand, it is also possible to realize the relic density of LSP neutralino smaller than the current bounds (Point 1 in Table 2, Points 1 and 2 in Table 3). If the dark matter relic density is saturated only by the LSP neutralino, then these points are also excluded by the current WMAP and Planck measurements. However, such solutions can be still available in conjunction with other form(s) of the dark matter [19,176]. In addition to the chargino-neutralino coannihilation scenario, Point 1 in Table 2 represents a solution in which stop is NLSP and nearly degenerate to the LSP neutralino in mass. Such solutions favor stop-neutralino coannihilation scenario. In Point 2 of Table 2, $m_A \simeq 2m_{\tilde{\chi}^0_1}$, and it is an $A-$resonance solution in which two LSP neutralinos annihilate into a $CP-$odd Higgs boson.

Since the Higgsino are rather heavy ($\mu \sim m_0$), they do not take part in forming the LSP neutralino; thus, the dark matter solutions yield small cross-sections for the dark matter scattering at nuclei. On the other hand, since the wino may mix with bino in the LSP neutralino, it may give some

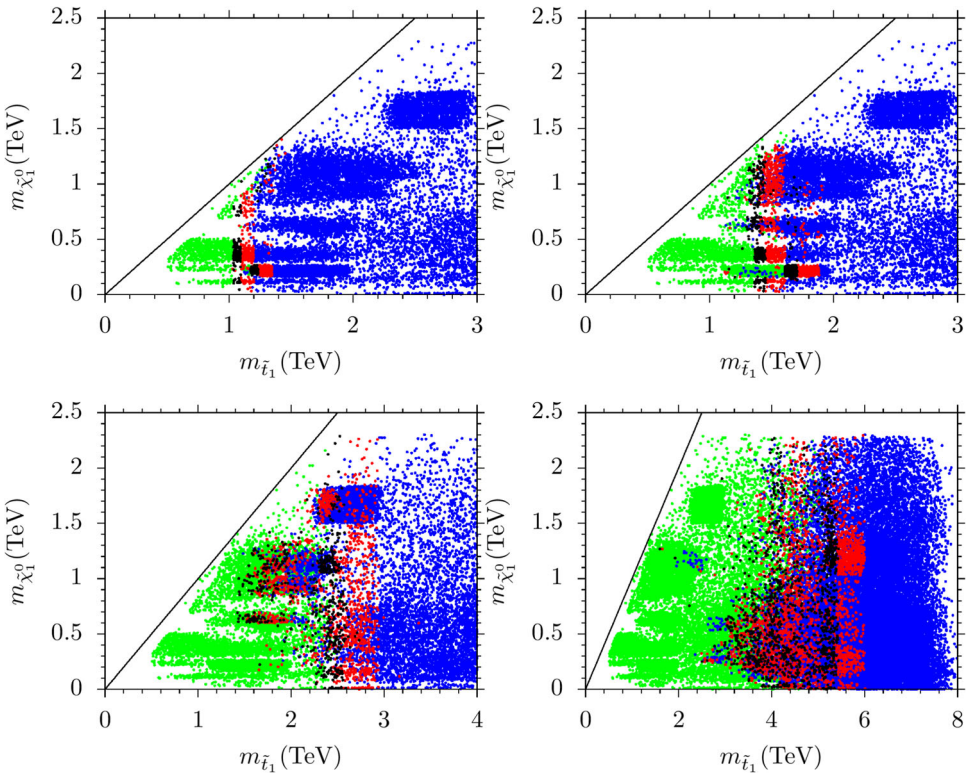

Fig. 10 Plots in the $m_{\tilde{\chi}_1^0} - m_{\tilde{t}_1}$ planes showing the combined signal strength of the three class of the signal processes in the same color coding as Fig. 5 for the experiments of 14 TeV (top left), 27 TeV (top right), 100 TeV (bottom) center of mass energies with 36.1 fb^{-1} luminosity. The bottom right panel shows the results for the 100 TeV center of mass energy with 3000 fb^{-1} luminosity

enhancement to the scattering cross-section. In this context, some of the solutions represented in our work can potentially be tested in dark matter direct detection experiments, as well. We present the results for dark matter scattering cross-section in comparison with the current and future projected exclusion curves from several direct detection experiments in Fig. 11. Even though the spin-independent cross-section results are mostly below the current and projected experimental results, there are some solutions placed between the current and projected LUX-Zeplin results. Such solutions are expected to be tested in direct detection experiments in near future. On the other hand, the spin-dependent scattering results are way below the current and projected experimental exclusion curves, and the solutions should wait for further upgrades in the ongoing experiments to be tested. Before concluding, we should note that since our scans are devoted to the collider analyses, the statistics for the direct dark matter experiments are rather able to give some rough results. More thorough scans may display more solutions between the current and projected curves, which will be tested soon.

Besides, we assume the relic density of the dark matter to be saturated only by the LSP neutralino, and this condition yields a strong impact on the solutions. As seen from the left panel in Fig. 11, there are green points around the current exclusion curve from the LUX-Zeplin experiment within 2σ uncertainty. Even though these solutions do not satisfy the relic density constraint from the measurements of the WMAP and Planck satellites due to our assumption, as we mentioned above, they may still be available in conjunction with other form(s) of dark matter and they can be tested within more thorough dark matter analyses. This approach, on the other hand, does not resolve the issue for the solutions yielding large relic density for neutralino (see, for instance, Point 2 in Table 2). Such solutions can be accommodated into models where the mass spectrum involves another LSP such as right-handed sneutrino or gravitino, while neutralino happens to be NLSP. The existence of these LSPs brings stronger constraints on the supersymmetric particles such as stau, stop, gluino etc. Since these particles interact with the LSP very weakly, they can escape from the detector, and this escape should be noticed as the missing color/charge in the final state of the events, when these particles are realized as NLSP. Thus, neutralino NLSP solutions are safe for the collider analyses, while they can be strictly constrained by the dark matter analyses. In this context, we also present solutions with incompatible density of neutralino, since such solutions can still be accommodated in models, and available for the collider experiments and analyses.

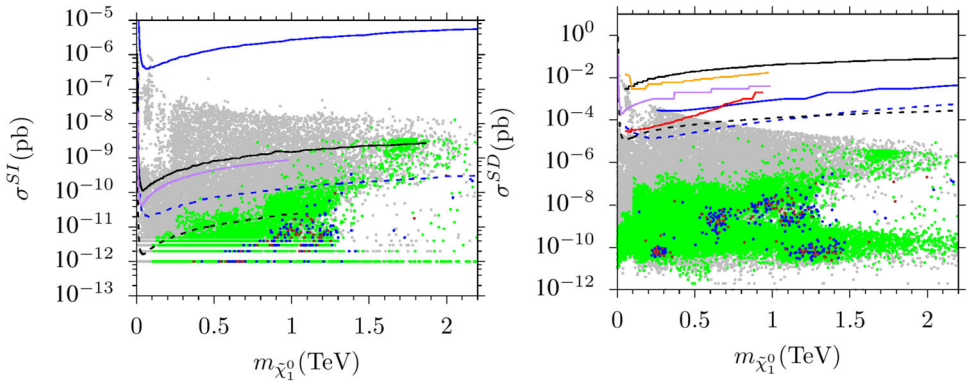

Fig. 11 The Spin-independent and Spin-dependent scattering cross-sections of the dark matter. All points are compatible with the REWSB and LSP neutralino conditions. Green points are allowed by the mass bounds and constraints from rare $B-$meson decays. Blue and brown points are subsets of green, and they satisfy, respectively, the WMAP and Planck bounds on the relic abundance of LSP neutralino within 5σ. In the $\sigma^{SI} - m_{\tilde{\chi}_1^0}$ plane, the blue solid (dashed) curve represents the current (projected) results of the CDMS experiment [206], while the black solid (dashed) curve is the current (projected) exclusion from the LUX-Zeplin experiment [207]. The magenta curve shows the results from the XENON-1T [208]. In the $\sigma^{SD} - m_{\tilde{\chi}_1^0}$ plane, the black solid (dashed) curve shows the current (projected) results from the LUX-Zeplin experiment [209], the orange curve is from the SuperKamiokande experiment [210]. The magenta curve represents the results from XENON-1T [211], while the red curve is obtained from the collider experiments [212]. Finally, the blue solid (dashed) curve is the current (projected) results from the IceCube/DeepCore experiment

6 Conclusion

We have discussed the stop masses and possible signal process within a class of SUSY GUTs with non-universal gaugino masses. This class of models predicts the stop mass in a wide range from about 400 GeV to 8 TeV, and the DM constraints yield a further lower bound on the stop mass as $m_{\tilde{t}_1} \gtrsim 500$ GeV. The mass spectrum also includes the gluino mass from 2.1 TeV (as stated by the gluino mass bound) to beyond 10 TeV. It usually happens to be heavier than the stop, despite the presence of a very narrow region in which the stop can slightly be heavier than gluino. However, this region is excluded by the DM constraints. The LSP neutralino always takes part in possible signal processes, and its mass is realized as heavy as about 2.3 TeV in the fundamental parameter space. Even though LHC allowed region allows almost massless neutralino, the DM constraints bounds its mass at about 200 GeV from below. Similarly the lightest chargino mass can be realized beyond 3 TeV, while the DM constraints bound its mass at about 2.7 TeV from above.

We consider three possible signal processes to probe the stop in this class of SUSY GUTs. The strongest impact can be obtained when a stop significantly decays into a LSP neutralino along with a top quark, which we refer to Signal 1. The current experiments at 14 TeV center of mass energy with 36.1 fb^{-1} luminosity can exclude the stop mass up to about 1.2 TeV through this decay channel, while the stop mass can be expected to be probed up to about 1.6 TeV in the experiments with 27 TeV center of mass energy, while the probe scale will raise to about 3 TeV when the 100 TeV center of mass energy is set in the collider experiments. If 3000 fb^{-1} luminosity is reached in 100 TeV collider experiments, this channel can probe the stop mass up to about 6 TeV. Another decay mode of the stop can be listed as Signal 2, in which it decays into a bottom quark along with a chargino, and the chargino successively decays into a $W-$boson and LSP neutralino. We found that this channel is not available for the current collider experiments, since the lightest stop mass eigenstate is formed mostly by the right-handed stop in this class of SUSY GUTs. Only a small region with $0.8 \lesssim m_{\tilde{t}_1} \lesssim 1.2$ TeV can yield a considerable left-handed stop mixing, and it leads to a visible signal. Despite the lack of good statistics for the current experiments, this channel can be expected to be available and probe the stop mass to about 4.8 TeV in the experiments with 100 TeV center of mass energy and 3000 fb^{-1} luminosity. However, a similar signal can be considered in which the chargino's successive decay is into two quarks and a LSP neutralino, which is stated as Signal 3 in our discussion. Similar analyses have revealed that this channel is available for the current experiments, and it excludes the solutions with $m_{\tilde{t}_1} \lesssim 1.2$. It provides also a promising signal through which the stop mass can be probed to about 2 TeV at 27 TeV, and 2.8 TeV at 100 TeV center of mass energies. Besides, high luminosity lifts the probing scale for the stop mass up to about 5 TeV. These results are applicable when the stop decays follow the signal processes under concern. The solutions with $SS < 1$ (shown in blue) mean the signal process considered is not strong enough to be tested and/or probed. As discussed over the tables of benchmark points, such solutions might be tested through different signal processes, and they may bound and probe the stop at different mass scales.

The solutions with $SS < 1$ (shown in blue) mean that a signal process considered is not strong enough to be tested and/or probed. On the other hand, such solutions may yield visible signals if one considers different processes. In this context, we also present combined results for the strength of all the three signals. The current experiments can exclude the region with $m_{\tilde{t}_1} \lesssim 1$ TeV in this class of $SO(10)$ models, since all solutions in this region yield $SS > 3$. The experiments with 27 TeV center of mass energy can be eligible to probe the stop mass up to about 1.4 TeV. However, one can still identify a few blue points in the region with $m_{\tilde{t}_1} \lesssim 1.4$ TeV. Such solutions predict the Wino-like LSP neutralino, and the $SU(2)_L$ interactions are suppressed due to the right-handedness of the lightest stop mass eigenstate. The experiments with 100 TeV center of mass energy can probe the stop mass up to about 3 TeV, and 6 TeV when a high luminosity is obtained. We identified some solutions which yield weak signal strength despite the high center of mass energy and luminosity. These solutions predict the gluino to be lighter than stop, and they can be tested through different signal processes such as $\tilde{t}_1 \to \tilde{g}t$.

Acknowledgements The work of Z. A, Z. K. and C. S. U is supported by the Scientific and Technological Research Council of Turkey (TUBITAK) Grant No. MFAG-118F090. Part of the calculations reported in this paper were performed at the National Academic Network and Information Center (ULAKBIM) of TUBITAK, High Performance and Grid Computing Center (TRUBA Resources).

Data Availability Statement This manuscript has no associated data or the data will not be deposited. [Author's comment: The raw data were generated in a large scale by employing publicly available computational packages, which have been made available within citations.]

Funded by SCOAP[3].

References

1. G. Aad et al., ATLAS Collaboration, Phys. Lett. B **716**, 1–29 (2012)
2. S. Chatrchyan et al., CMS Collaboration, JHEP **1306**, 081 (2013)
3. E. Gildener, Phys. Rev. D **14**, 1667 (1976)
4. E. Gildener, Phys. Lett. B **92**, 111 (1980)
5. S. Weinberg, Phys. Lett. B **82**, 387 (1979)
6. L. Susskind, Phys. Rev. D **20**, 2619 (1979)
7. M.J.G. Veltman, Acta Phys. Polon. B **12**, 437 (1981)
8. G. Degrassi, S. Di Vita, J. Elias-Miro, J.R. Espinosa, G.F. Giudice, G. Isidori, A. Strumia, JHEP **1208**, 098 (2012). arXiv:1205.6497 [hep-ph]
9. F. Bezrukov, M.Y. Kalmykov, B.A. Kniehl, M. Shaposhnikov, JHEP **1210**, 140 (2012). arXiv:1205.2893 [hep-ph]
10. D. Buttazzo, G. Degrassi, P.P. Giardino, G.F. Giudice, F. Sala, A. Salvio, A. Strumia, JHEP **1312**, 089 (2013). arXiv:1307.3536
11. U. Chattopadhyay, P. Nath, Phys. Rev. D **65**, 075009 (2002)
12. S. Komine, M. Yamaguchi, Phys. Rev. D **65**, 075013 (2002)
13. S. Profumo, Phys. Rev. D **68**, 015006 (2003)
14. C. Pallis, Nucl. Phys. B **678**, 398 (2004)
15. C. Balazs, R. Dermisek, JHEP **0306**, 024 (2003)
16. W. Altmannshofer, D. Guadagnoli, S. Raby, D.M. Straub, Phys. Lett. B **668**, 385 (2008)
17. I. Gogoladze, R. Khalid, N. Okada, Q. Shafi, Phys. Rev. D **79**, 095022 (2009)
18. S. Antusch, M. Spinrath, Phys. Rev. D **79**, 095004 (2009)
19. H. Baer, I. Gogoladze, A. Mustafayev, S. Raza, Q. Shafi, JHEP **1203**, 047 (2012). arXiv:1201.4412 [hep-ph]
20. I. Gogoladze, R. Khalid, S. Raza, Q. Shafi, JHEP **1012**, 055 (2010). arXiv:1008.2765 [hep-ph]
21. S. Raza, Q. Shafi, C.S. Un, JHEP **1905**, 046 (2019). arXiv:1812.10128 [hep-ph]
22. B. Ananthanarayan, G. Lazarides, Q. Shafi, Phys. Rev. D **44**, 1613 (1991)
23. B. Ananthanarayan, G. Lazarides, Q. Shafi, Phys. Lett. B **300**(24), 5 (1993)
24. Q. Shafi, B. Ananthanarayan, Trieste HEP Cosmol. 233–244 (1991)
25. V. Barger, M. Berger, P. Ohmann, Phys. Rev. D **49**, 4908 (1994)
26. M. Carena, M. Olechowski, S. Pokorski, C. Wagner, Nucl. Phys. B **426**, 269 (1994)
27. B. Ananthanarayan, Q. Shafi, X. Wang, Phys. Rev. D **50**, 5980 (1994)
28. G. Anderson et al., Phys. Rev. D **47**, 3702 (1993)
29. G. Anderson et al., Phys. Rev. D **49**, 3660 (1994)
30. R. Rattazzi, U. Sarid, Phys. Rev. D **53**, 1553 (1996)
31. T. Blazek, M. Carena, S. Raby, C. Wagner, Phys. Rev. D **56**, 6919 (1997)
32. T. Blazek, S. Raby, K. Tobe, Phys. Rev. D **62**, 055001 (2000)
33. H. Baer, M. Diaz, J. Ferrandis, X. Tata, Phys. Rev. D **61**, 111701 (2000)
34. H. Baer, M. Brhlik, M. Diaz, J. Ferrandis, P. Mercadante, P. Quintana, X. Tata, Phys. Rev. D **63**, 015007 (2001)
35. S. Profumo, Phys. Rev. D **68**, 015006 (2003)
36. C. Balazs, R. Dermisek, JHEP **0306**, 024 (2003)
37. C. Pallis, Nucl. Phys. B **678**, 398 (2004)
38. M. Gomez, G. Lazarides, C. Pallis, Phys. Rev. D **61**, 123512 (2000)
39. M. Gomez, G. Lazarides, C. Pallis, Nucl. Phys. B **638**, 165 (2002)
40. M. Gomez, G. Lazarides, C. Pallis, Phys. Rev. D **67**, 097701 (2003)
41. I. Gogoladze, Y. Mimura, S. Nandi, K. Tobe, Phys. Lett. B **575**, 66 (2003)
42. U. Chattopadhyay, A. Corsetti, P. Nath, Phys. Rev. D **66**, 035003 (2002)
43. T. Blazek, R. Dermisek, S. Raby, Phys. Rev. Lett. **88**, 111804 (2002)
44. T. Blazek, R. Dermisek, S. Raby, Phys. Rev. D **65**, 115004 (2002)
45. M. Gomez, T. Ibrahim, P. Nath, S. Skadhauge, Phys. Rev. D **72**, 095008 (2005)
46. K. Tobe, J.D. Wells, Nucl. Phys. B **663**, 123 (2003)
47. W. Altmannshofer, D. Guadagnoli, S. Raby, D.M. Straub, Phys. Lett. B **668**, 385 (2008)
48. D. Guadagnoli, S. Raby, D.M. Straub, JHEP **0910**, 059 (2009)

49. H. Baer, S. Kraml, S. Sekmen, JHEP **0909**, 005 (2009)
50. K. Choi, D. Guadagnoli, S.H. Im, C.B. Park, arXiv:1005.0618 [hep-ph]
51. B. Dutta, Y. Mimura, arXiv:1810.08413 [hep-ph]
52. S. Raza, Q. Shafi, C. S. Ün, Phys. Rev. D **92**(5), 055010 (2015). arXiv:1412.7672 [hep-ph]
53. The ATLAS collaboration [ATLAS Collaboration], ATLAS-CONF-2019-004
54. The ATLAS collaboration [ATLAS Collaboration], ATLAS-CONF-2018-002
55. V. Khachatryan et al., CMS Collaboration, JHEP **1510**, 144 (2015). arXiv:1504.00936 [hep-ex]
56. G. Aad et al. [ATLAS Collaboration], Phys. Rev. D **92**(1), 012006 (2015). arXiv:1412.2641 [hep-ex]
57. G. Aad et al., ATLAS Collaboration, JHEP **1508**, 137 (2015). arXiv:1506.06641 [hep-ex]
58. S. Chatrchyan et al., CMS Collaboration, JHEP **1401**, 096 (2014). arXiv:1312.1129 [hep-ex]
59. A. M. Sirunyan et al. [CMS Collaboration], Phys. Rev. Lett. **120**(7), 071802 (2018). arXiv:1709.05543 [hep-ex]
60. The ATLAS collaboration [ATLAS Collaboration], ATLAS-CONF-2017-047
61. The ATLAS collaboration [ATLAS Collaboration], ATLAS-CONF-2018-004
62. A. M. Sirunyan et al. [CMS Collaboration], Phys. Rev. Lett. **121**(12), 121801 (2018). arXiv:1808.08242 [hep-ex]
63. See, for instance, G. Aad et al. [ATLAS Collaboration], arXiv:1907.02749 [hep-ex]
64. The ATLAS collaboration [ATLAS Collaboration], ATLAS-CONF-2019-010
65. CMS Collaboration [CMS Collaboration], CMS-PAS-HIG-17-033
66. CMS Collaboration [CMS Collaboration], CMS-PAS-HIG-18-023
67. A.M. Sirunyan et al., CMS Collaboration, Eur. Phys. J. C **79**, 564 (2019). arXiv:1903.00941 [hep-ex]
68. A. M. Sirunyan et al. [CMS Collaboration], arXiv:1905.07453 [hep-ex]
69. CMS Collaboration [CMS Collaboration], CMS-PAS-HIG-18-020
70. A.M. Sirunyan et al., CMS Collaboration, JHEP **1811**, 161 (2018). arXiv:1808.01890 [hep-ex]
71. A.M. Sirunyan et al., CMS Collaboration, JHEP **1711**, 010 (2017). arXiv:1707.07283 [hep-ex]
72. P. Ko, J. Li, C. Yu, arXiv:1610.07526 [hep-ph]
73. K. Lane, L. Pritchett, arXiv:1701.07376 [hep-ph]
74. V. Khachatryan et al., CMS Collaboration, Phys. Lett. B **749**, 337 (2015). arXiv:1502.07400 [hep-ex]
75. G. Aad et al., ATLAS Collaboration, JHEP **1511**, 211 (2015). arXiv:1508.03372 [hep-ex]
76. W. Abdallah, A. Hammad, S. Khalil, S. Moretti, Phys. Lett. B **788**, 65 (2019). arXiv:1806.03585 [hep-ph]
77. W. Abdallah, A. Hammad, S. Khalil, S. Moretti, Phys. Rev. D **95**(5), 055019 (2017). arXiv:1608.07500 [hep-ph]
78. A. Hammad, S. Khalil, C. S. Un, Phys. Rev. D **95**(5), 055028 (2017). arXiv:1605.07567 [hep-ph]
79. M.E. Gomez, S. Heinemeyer, M. Rehman, arXiv:1703.02229 [hep-ph]
80. S. Fathy, T. Ibrahim, A. Itani, P. Nath, Phys. Rev. D **94**(11), 115029 (2016). arXiv:1608.05998 [hep-ph]
81. P. Athron, J. H. Park, T. Steudtner, D. Stöckinger, A. Voigt, JHEP **1701**, 079 (2017). arXiv:1609.00371 [hep-ph]
82. J. Ellis, J. Quevillon, V. Sanz, JHEP **1610**, 086 (2016). arXiv:1607.05541 [hep-ph]
83. C. Beskidt, W. de Boer, D.I. Kazakov, S. Wayand, Phys. Lett. B **759**, 141 (2016). arXiv:1602.08707 [hep-ph]
84. B. Bhattacherjee, M. Chakraborti, A. Chakraborty, U. Chattopadhyay, D. Das, D.K. Ghosh, Phys. Rev. D **88**(3), 035011 (2013). arXiv:1305.4020 [hep-ph]
85. T. A. Vami [ATLAS and CMS], PoS **LHCP2019**, 168 (2019). https://doi.org/10.22323/1.350.0168. arXiv:1909.11753 [hep-ex]
86. G. Aad et al. [ATLAS], arXiv:1909.08457 [hep-ex]
87. Z. Altin, A. Cici, Z. Kirca, Q. Shafi, C.S. Un, arXiv:1910.01457 [hep-ph]
88. T. A. Vami [ATLAS and CMS Collaborations], arXiv:1909.11753 [hep-ex]
89. J. Mitrevski [ATLAS Collaboration], PoS DIS **2018**, 079 (2018)
90. C. Collard [CMS Collaboration], arXiv:1709.00868 [hep-ex]
91. The ATLAS collaboration [ATLAS Collaboration], ATLAS-CONF-2016-077
92. M.A. Ajaib, T. Li, Q. Shafi, Phys. Rev. D **85**, 055021 (2012). arXiv:1111.4467 [hep-ph]
93. A.M. Sirunyan et al., CMS Collaboration, JHEP **1710**, 005 (2017). arXiv:1707.03316 [hep-ex]
94. D.A. Demir, C.S. Un, Phys. Rev. D **90**, 095015 (2014). arXiv:1407.1481 [hep-ph]
95. A. Çiçi, Z. Kırca, C.S. Un, Eur. Phys. J. C **78**(1), 60 (2018). arXiv:1611.05270 [hep-ph], and references therein
96. M. Abud, F. Buccella, Int. J. Mod. Phys. A **16**, 609–624 (2001). https://doi.org/10.1142/S0217751X01003056. arXiv:hep-ph/0006029 [hep-ph]
97. K. Bora, G. Ghosh, J. Phys: Conf. Ser. **481**, 012016 (2014). https://doi.org/10.1088/1742-6596/481/1/012016
98. B. Bajc, G. Senjanovic, F. Vissani, Phys. Rev. D **70**, 093002 (2004). https://doi.org/10.1103/PhysRevD.70.093002. arXiv:hep-ph/0402140 [hep-ph]
99. M. Chakraborty, M. Parida, B. Sahoo, JCAP **01**, 049 (2020). https://doi.org/10.1088/1475-7516/2020/01/049. arXiv:1906.05601 [hep-ph]
100. T. Fukuyama, N. Okada, Mod. Phys. Lett. A **33**(29), 1850167 (2018). https://doi.org/10.1142/S0217732318501675. arXiv:1802.06530 [hep-ph]
101. Z. Ren, D. Zhang, Eur. Phys. J. Plus **132**(7), 322 (2017). https://doi.org/10.1140/epjp/i2017-11597-2. arXiv:1704.03959 [hep-ph]
102. L. Calibbi, D. Chowdhury, A. Masiero, K. Patel, S. Vempati, JHEP **11**, 040 (2012). https://doi.org/10.1007/JHEP11(2012)040. arXiv:1207.7227 [hep-ph]
103. P. Bhupal Dev, R. Mohapatra, M. Severson, Phys. Rev. D **84**, 053005 (2011). https://doi.org/10.1103/PhysRevD.84.053005. arXiv:1107.2378 [hep-ph]
104. M. Fukugita, T. Yanagida, Phys. Lett. B **174**, 45–47 (1986). https://doi.org/10.1016/0370-2693(86)91126-3
105. G. Lazarides, Q. Shafi, Phys. Lett. B **258**, 305–309 (1991). https://doi.org/10.1016/0370-2693(91)91090-I
106. F. Buccella, D. Falcone, F. Tramontano, Phys. Lett. B **524**, 241–244 (2002). https://doi.org/10.1016/S0370-2693(01)01409-5. arXiv:hep-ph/0108172 [hep-ph]
107. P. Gu, U. Sarkar, Phys. Lett. B **663**, 80–82 (2008). https://doi.org/10.1016/j.physletb.2008.04.001. arXiv:0711.2727 [hep-ph]
108. M. K. Parida, R. Samantaray, arXiv:2002.06869 [hep-ph]
109. S. Saad, Nucl. Phys. B **943**, 114630 (2019). https://doi.org/10.1016/j.nuclphysb.2019.114630. arXiv:1712.04880 [hep-ph]
110. M. Pernow,
111. S. Mandal, R. Srivastava, J. W. Valle, arXiv:1903.03631 [hep-ph]
112. K. Agashe, P. Du, M. Ekhterachian, C.S. Fong, S. Hong, L. Vecchi, JHEP **04**, 029 (2019). https://doi.org/10.1007/JHEP04(2019)029. arXiv:1812.08204 [hep-ph]
113. M. Abbas, S. Khalil, JHEP **04**, 056 (2008). https://doi.org/10.1088/1126-6708/2008/04/056. arXiv:0707.0841 [hep-ph]
114. R. Mohapatra, J. Valle, Phys. Rev. D **34**, 1642 (1986). https://doi.org/10.1103/PhysRevD.34.1642

115. M. Gonzalez-Garcia, J. Valle, Phys. Lett. B **216**, 360–366 (1989). https://doi.org/10.1016/0370-2693(89)91131-3
116. S. Khalil, Phys. Rev. D **82**, 077702 (2010). https://doi.org/10.1103/PhysRevD.82.077702. arXiv:1004.0013 [hep-ph]
117. Z. Altın, Ö. Özdal, C.S. Un, Phys. Rev. D **97**(5), 055007 (2018). https://doi.org/10.1103/PhysRevD.97.055007. arXiv:1703.00229 [hep-ph]
118. P. Langacker, Phys. Rept. **72**, 185 (1981). https://doi.org/10.1016/0370-1573(81)90059-4
119. K. Babu, R. Mohapatra, Phys. Rev. Lett. **70**, 2845–2848 (1993). https://doi.org/10.1103/PhysRevLett.70.2845. arXiv:hep-ph/9209215 [hep-ph]
120. G. Anderson, S. Raby, S. Dimopoulos, L. Hall, G. Starkman, Phys. Rev. D **49**, 3660–3690 (1994). https://doi.org/10.1103/PhysRevD.49.3660. arXiv:hep-ph/9308333 [hep-ph]
121. M. Drees, Phys. Lett. B **181**, 279–282 (1986). https://doi.org/10.1016/0370-2693(86)90046-8
122. Y. Kawamura, H. Murayama, M. Yamaguchi, Phys. Lett. B **324**, 52–58 (1994). https://doi.org/10.1016/0370-2693(94)00107-3. arXiv:hep-ph/9402254 [hep-ph]
123. C.F. Kolda, S.P. Martin, Phys. Rev. D **53**, 3871–3883 (1996). https://doi.org/10.1103/PhysRevD.53.3871. arXiv:hep-ph/9503445 [hep-ph]
124. D. Miller, A. Morais, P. Pandita, Phys. Rev. D **87**(1), 015007 (2013). https://doi.org/10.1103/PhysRevD.87.015007. arXiv:1208.5906 [hep-ph]
125. K. Babu, T. Enkhbat, B. Mukhopadhyaya, Nucl. Phys. B **720**, 47–63 (2005). https://doi.org/10.1016/j.nuclphysb.2005.05.006. arXiv:hep-ph/0501079 [hep-ph]
126. G. Dvali, S. Pokorski, Phys. Lett. B **379**, 126–134 (1996). https://doi.org/10.1016/0370-2693(96)00357-7. arXiv:hep-ph/9601358 [hep-ph]
127. R. Rattazzi, U. Sarid, Phys. Rev. D **53**, 1553–1585 (1996). https://doi.org/10.1103/PhysRevD.53.1553. arXiv:hep-ph/9505428 [hep-ph]
128. K. Babu, B. Bajc, S. Saad, JHEP **02**, 136 (2017). https://doi.org/10.1007/JHEP02(2017)136. arXiv:1612.04329 [hep-ph]
129. M. Ciuchini, V. Lubicz, L. Conti, A. Vladikas, A. Donini, E. Franco, G. Martinelli, I. Scimemi, V. Gimenez, L. Giusti, A. Masiero, L. Silvestrini, M. Talevi, JHEP **10**, 008 (1998). https://doi.org/10.1088/1126-6708/1998/10/008. arXiv:hep-ph/9808328 [hep-ph]
130. K. Babu, I. Gogoladze, S. Raza, Q. Shafi, Phys. Rev. D **90**(5), 056001 (2014). https://doi.org/10.1103/PhysRevD.90.056001. arXiv:1406.6078 [hep-ph]
131. Y. Kawamura, H. Murayama, M. Yamaguchi, Phys. Rev. D **51**, 1337–1352 (1995). https://doi.org/10.1103/PhysRevD.51.1337. arXiv:hep-ph/9406245 [hep-ph]
132. K. Babu, S.M. Barr, Phys. Lett. B **387**, 87–98 (1996). https://doi.org/10.1016/0370-2693(96)01002-7. arXiv:hep-ph/9606384 [hep-ph]
133. A.H. Chamseddine, R.L. Arnowitt, P. Nath, Phys. Rev. Lett. **49**, 970 (1982). https://doi.org/10.1103/PhysRevLett.49.970
134. R. Barbieri, S. Ferrara, C.A. Savoy, Phys. Lett. B **119**, 343 (1982). https://doi.org/10.1016/0370-2693(82)90685-2
135. N. Ohta, Prog. Theor. Phys. **70**, 542 (1983). https://doi.org/10.1143/PTP.70.542
136. L.J. Hall, J.D. Lykken, S. Weinberg, Phys. Rev. D **27**, 2359–2378 (1983). https://doi.org/10.1103/PhysRevD.27.2359
137. Q. Shafi, C. Wetterich, Phys. Rev. Lett. **52**, 875 (1984). https://doi.org/10.1103/PhysRevLett.52.875
138. B. Ananthanarayan, P. Pandita, Int. J. Mod. Phys. A **22**, 3229–3259 (2007). https://doi.org/10.1142/S0217751X07036889. arXiv:0706.2560 [hep-ph]
139. S. Bhattacharya, A. Datta, B. Mukhopadhyaya, JHEP **10**, 080 (2007). https://doi.org/10.1088/1126-6708/2007/10/080. arXiv:0708.2427 [hep-ph]
140. S.P. Martin, Phys. Rev. D **79**, 095019 (2009). https://doi.org/10.1103/PhysRevD.79.095019. arXiv:0903.3568 [hep-ph]
141. U. Chattopadhyay, D. Das, D. Roy, Phys. Rev. D **79**, 095013 (2009). https://doi.org/10.1103/PhysRevD.79.095013. arXiv:0902.4568 [hep-ph]
142. A. Corsetti, P. Nath, Phys. Rev. D **64**, 125010 (2001). https://doi.org/10.1103/PhysRevD.64.125010. arXiv:hep-ph/0003186 [hep-ph]
143. Y. Hiçyılmaz, L. Selbuz, L. Solmaz, C.S. Ün, Phys. Rev. D **97**(11), 115041 (2018). https://doi.org/10.1103/PhysRevD.97.115041. arXiv:1711.07967 [hep-ph]
144. Y. Hiçyılmaz, L. Solmaz, Ş.H. Tanyıldızı, C.S. Ün, Nucl. Phys. B **933**, 275–298 (2018). https://doi.org/10.1016/j.nuclphysb.2018.05.025. arXiv:1706.04561 [hep-ph]
145. Y. Hiçyılmaz, M. Ceylan, A. Altas, L. Solmaz, C.S. Un, Phys. Rev. D **94**(9), 095001 (2016). https://doi.org/10.1103/PhysRevD.94.095001. arXiv:1604.06430 [hep-ph]
146. C.S. Un, O. Ozdal, Phys. Rev. D **93**, 055024 (2016). https://doi.org/10.1103/PhysRevD.93.055024. arXiv:1601.02494 [hep-ph]
147. L. Delle Rose, S. Khalil, S. King, J.D., S. Kulkarni, C. Marzo, S. Moretti, C.S. Un, JHEP **07**, 100 (2018). https://doi.org/10.1007/JHEP07(2018)100. arXiv:1712.05232 [hep-ph]
148. L. Delle Rose, S. Khalil, S.J.D. King, C. Marzo, S. Moretti, C.S. Un, Phys. Rev. D **96**(5), 055004 (2017). https://doi.org/10.1103/PhysRevD.96.055004. arXiv:1702.01808 [hep-ph]
149. S. Khalil, H. Okada, Phys. Rev. D **79**, 083510 (2009). https://doi.org/10.1103/PhysRevD.79.083510. arXiv:0810.4573 [hep-ph]
150. M. Frank, Ö. Özdal, Phys. Rev. D **97**(1), 015012 (2018). https://doi.org/10.1103/PhysRevD.97.015012. arXiv:1709.04012 [hep-ph]
151. R. Kappl, M. Ratz, M.W. Winkler, Phys. Lett. B **695**, 169–173 (2011). https://doi.org/10.1016/j.physletb.2010.10.063. arXiv:1010.0553 [hep-ph]
152. See, for instance, M. Chala, A. Delgado, G. Nardini, M. Quiros, JHEP **04**, 097 (2017). https://doi.org/10.1007/JHEP04(2017)097. arXiv:1702.07359 [hep-ph]
153. See, for instance, J. S. Kim, S. Pokorski, K. Rolbiecki, K. Sakurai, JHEP **09**, 082 (2019). https://doi.org/10.1007/JHEP09(2019)082. arXiv:1905.05648 [hep-ph]
154. G. Aad et al. [ATLAS], [arXiv:2003.11956 [hep-ex]]
155. [CMS], CMS-PAS-EXO-19-021
156. B. Bajc, S. Lavignac, T. Mede, JHEP **01**, 044 (2016). https://doi.org/10.1007/JHEP01(2016)044. arXiv:1509.06680 [hep-ph]
157. J. Hisano, D. Kobayashi, T. Kuwahara, N. Nagata, JHEP **07**, 038 (2013). https://doi.org/10.1007/JHEP07(2013)038. arXiv:1304.3651 [hep-ph]
158. W. Porod, Comput. Phys. Commun. **153**, 275 (2003)
159. W. Porod, F. Staub, Comput. Phys. Commun. **183**, 2458 (2012)
160. F. Staub, (2008). arXiv:0806.0538
161. F. Staub, Comput. Phys. Commun. **182**, 808 (2011)
162. J. Hisano, H. Murayama, T. Yanagida, Nucl. Phys. B **402**, 46 (1993)
163. J.L. Chkareuli, I.G. Gogoladze, Phys. Rev. D **58**, 055011 (1998)
164. T. E. W. Group [CDF and D0 Collaborations], (2009). arXiv:0903.2503
165. I. Gogoladze, R. Khalid, S. Raza, Q. Shafi, JHEP **1106**, 117 (2011)
166. I. Gogoladze, Q. Shafi, C.S. Un, JHEP **1208**, 028 (2012)
167. M. Adeel Ajaib, I. Gogoladze, Q. Shafi, C.S. Un, JHEP **07**, 139 (2013). https://doi.org/10.1007/JHEP07(2013)139. arXiv:1303.6964 [hep-ph]
168. L.E. Ibanez, G.G. Ross, Phys. Lett. B **110**, 215 (1982)
169. K. Inoue, A. Kakuto, H. Komatsu, S. Takeshita, Prog. Theor. Phys. **68**, 927 (1982)

170. L.E. Ibanez, Phys. Lett. B **118**, 73 (1982)
171. J.R. Ellis, D.V. Nanopoulos, K. Tamvakis, Phys. Lett. B **121**, 123 (1983)
172. L. Alvarez-Gaume, J. Polchinski, M.B. Wise, Nucl. Phys. B **221**, 495 (1983)
173. K. Nakamura et al., Particle Data Group Collaboration. J. Phys. G **37**, 075021 (2010)
174. G. Hinshaw et al., WMAP Collaboration, Astrophys. J. Suppl. **208**, 19 (2013). arXiv:1212.5226 [astro-ph.CO]
175. Y. Akrami et al. [Planck Collaboration], arXiv:1807.06205 [astro-ph.CO]
176. T. Li, D.V. Nanopoulos, S. Raza, X.C. Wang, JHEP **1408**, 128 (2014). arXiv:1406.5574 [hep-ph]
177. K.A. Olive et al., Particle Data Group Collaboration, Chin. Phys. C **38**, 090001 (2014)
178. R. Aaij et al., LHCb Collaboration, Phys. Rev. Lett. **110**(2), 021801 (2013)
179. Y. Amhis, et al. [Heavy Flavor Averaging Group Collaboration], (2012). arXiv:1207.1158
180. D. Asner, et al. [Heavy Flavor Averaging Group Collaboration], (2010). arXiv:1010.1589
181. A. Vicente, Nucl. Part. Phys. Proc. **273–275**, 1423–1428 (2016). https://doi.org/10.1016/j.nuclphysbps.2015.09.230. arXiv:1410.2099 [hep-ph]
182. A.J. Buras, J. Girrbach, D. Guadagnoli, G. Isidori, Eur. Phys. J. C **72**, 2172 (2012). https://doi.org/10.1140/epjc/s10052-012-2172-1. arXiv:1208.0934 [hep-ph]
183. M. Misiak, H. Asatrian, R. Boughezal, M. Czakon, T. Ewerth, A. Ferroglia, P. Fiedler, P. Gambino, C. Greub, U. Haisch, T. Huber, M. Kaminski, G. Ossola, M. Poradzinski, A. Rehman, T. Schutzmeier, M. Steinhauser, J. Virto, Phys. Rev. Lett. **114**(22), 221801 (2015). https://doi.org/10.1103/PhysRevLett.114.221801. arXiv:1503.01789 [hep-ph]
184. M. Czakon, P. Fiedler, T. Huber, M. Misiak, T. Schutzmeier, M. Steinhauser, JHEP **04**, 168 (2015). https://doi.org/10.1007/JHEP04(2015)168. arXiv:1503.01791 [hep-ph]
185. S. P. Martin, Adv. Ser. Direct. High Energy Phys. **21**, 1–153 (2010). arXiv:hep-ph/9709356 [hep-ph]. (we kindly request also look at the discussion in the first paragraph of page 109)
186. G. Degrassi, S. Heinemeyer, W. Hollik, P. Slavich, G. Weiglein, Eur. Phys. J. C **28**, 133–143 (2003). https://doi.org/10.1140/epjc/s2003-01152-2. arXiv:hep-ph/0212020 [hep-ph]
187. H. Bahl, S. Heinemeyer, W. Hollik, G. Weiglein, arXiv:1912.04199 [hep-ph]
188. E. Bagnaschi, J. Pardo Vega, P. Slavich, Eur. Phys. J. C **77**(5), 334 (2017). https://doi.org/10.1140/epjc/s10052-017-4885-7. arXiv:1703.08166 [hep-ph]
189. B. Allanach, A. Djouadi, J. Kneur, W. Porod, P. Slavich, JHEP **09**, 044 (2004). https://doi.org/10.1088/1126-6708/2004/09/044. arXiv:hep-ph/0406166 [hep-ph]
190. P. Drechsel, R. Gröber, S. Heinemeyer, M.M. Muhlleitner, H. Rzehak, G. Weiglein, Eur. Phys. J. C **77**(6), 366 (2017). https://doi.org/10.1140/epjc/s10052-017-4932-4. arXiv:1612.07681 [hep-ph]
191. F. Staub, W. Porod, Eur. Phys. J. C **77**(5), 338 (2017). https://doi.org/10.1140/epjc/s10052-017-4893-7. arXiv:1703.03267 [hep-ph]
192. B. Allanach, A. Bednyakov, R. Ruiz de Austri, Comput. Phys. Commun. **189**, 192–206 (2015). https://doi.org/10.1016/j.cpc.2014.12.006. arXiv:1407.6130 [hep-ph]
193. P. Bergeron, P. Sandick, K. Sinha, JHEP **05**, 113 (2018). https://doi.org/10.1007/JHEP05(2018)113. arXiv:1712.05491 [hep-ph]
194. M. W. Cahill-Rowley, J. L. Hewett, A. Ismail, M. E. Peskin, T. G. Rizzo, arXiv:1305.2419 [hep-ph]
195. G. Belanger, F. Boudjema, A. Pukhov, R.K. Singh, JHEP **0911**, 026 (2009)
196. H. Baer, S. Kraml, S. Sekmen, H. Summy, JHEP **0803**, 056 (2008)
197. G. Belanger, F. Boudjema, A. Pukhov, A. Semenov, Comput. Phys. Commun. **176**, 367 (2007). arXiv:hep-ph/0607059
198. G. Belanger, F. Boudjema, A. Pukhov, A. Semenov, Comput. Phys. Commun. **185**, 960 (2014). arXiv:1305.0237 [hep-ph]
199. J. Alwall, M. Herquet, F. Maltoni, O. Mattelaer, T. Stelzer, JHEP **1106**, 128 (2011). arXiv:1106.0522 [hep-ph]
200. M. Muhlleitner, E. Popenda, JHEP **1104**, 095 (2011). arXiv:1102.5712 [hep-ph]
201. The ATLAS collaboration [ATLAS Collaboration], ATLAS-CONF-2013-068
202. W. Beenakker, M. Kramer, T. Plehn, M. Spira, P.M. Zerwas, Nucl. Phys. B **515**, 3 (1998). https://doi.org/10.1016/S0550-3213(98)00014-5. arXiv: hep-ph/9710451
203. K. Cranmer, https://doi.org/10.5170/CERN-2015-001.247., https://doi.org/10.5170/CERN-2014-003.267. arXiv:1503.07622 [physics.data-an]
204. U. Ellwanger, C. Hugonie, Phys. Lett. B **457**, 299–306 (1999). https://doi.org/10.1016/S0370-2693(99)00546-8. arXiv:hep-ph/9902401 [hep-ph]
205. See, for instance, H. Baer, V. Barger, J. S. Gainer, P. Huang, M. Savoy, D. Sengupta, X. Tata, Eur. Phys. J. C **77**(7), 499 (2017). arXiv:1612.00795 [hep-ph]
206. P. L. Brink et al. [CDMS-II], eConf **C041213**, 2529 (2004). arXiv:astro-ph/0503583 [astro-ph]
207. D. Akerib et al. [LUX-ZEPLIN], Phys. Rev. D **101**(5), 052002 (2020). https://doi.org/10.1103/PhysRevD.101.052002. arXiv:1802.06039 [astro-ph.IM]
208. E. Aprile et al. [XENON], Phys. Rev. Lett. **121**(11), 111302 (2018). https://doi.org/10.1103/PhysRevLett.121.111302. arXiv:1805.12562 [astro-ph.CO]
209. D. Akerib et al. [LUX], Phys. Rev. Lett. **116**(16), 161302 (2016). https://doi.org/10.1103/PhysRevLett.116.161302. arXiv:1602.03489 [hep-ex]
210. T. Tanaka et al. [Super-Kamiokande], Astrophys. J. **742**, 78 (2011). https://doi.org/10.1088/0004-637X/742/2/78. arXiv:1108.3384 [astro-ph.HE]
211. E. Aprile et al. [XENON], Phys. Rev. Lett. **122**(14), 141301 (2019). https://doi.org/10.1103/PhysRevLett.122.141301. arXiv:1902.03234 [astro-ph.CO]
212. V. Khachatryan et al. [CMS], Eur. Phys. J. C **75**(5), 235 (2015). https://doi.org/10.1140/epjc/s10052-015-3451-4. arXiv:1408.3583 [hep-ex]